

ACICULAR FERRITE AND BAINITE
IN
Fe-Cr-C WELD DEPOSITS

by

Sudarsanam Suresh Babu

Darwin College

Cambridge

A dissertation submitted for the degree of

Doctor of Philosophy

at the University of Cambridge

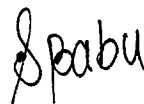
September 1991

To my mother
Smt. S. Rajalakshmi

PREFACE

This dissertation is submitted for the degree of Doctor of Philosophy at the University of Cambridge. It describes the work carried out under the supervision of Dr. H. K. D. H. Bhadeshia in the Department of Materials Science and Metallurgy, Cambridge, between October 1988 and September 1991. Except where appropriately referenced, this work is entirely original, and contains nothing which is the outcome of collaboration. No part of this dissertation has been, or is concurrently being, submitted for any other degree, diploma or any other qualification. It does not exceed 60,000 words in length.

Parts of this dissertation have been published in *Materials Science and Technology*, Vol. 6, 1990, pp. 1005-1020, *Materials Science and Engineering*, Vol. A142, 1991, pp. 209-219 and in *Materials Transactions, Japan Institute of Metals*, Vol. 32, 1991, pp. 679-688.



Suresh Babu S.

September, 1991.

ACKNOWLEDGEMENTS

I am grateful to the Cambridge Commonwealth Trust for the Scholarship and to the Council of Vice-Chancellors of the Universities in the the U.K. for the ORS award, for this research study. I am also grateful to ESAB (Sweden) and ESAB (UK) for the financial support and the welds used in the study. Thanks are also due to Prof. D. Hull and Prof. Colin Humphreys for providing the laboratory facilities in Cambridge.

I take this opportunity to express my sincere gratitude to Dr H. K. D. H. Bhadeshia for his continued guidance, encouragement and support through out this period of investigation. I have benefited from his extensive knowledge in phase transformations. His ability for always being "excited" about the results of this research, has led to better understanding. I am grateful to Dr Lars-Erik Svensson for his interest and encouragement. I thank Dr. H. Harada and Dr A. L. Greer for their valuable guidance concerning my research career.

Over the last three years, the phase transformations group have contributed greatly to my enjoyment of life. I will cherish those excellent "Darwin College Lunch Time" discussions on research outlook, which I am sure will act as a guiding light for me in the years to come. I have been also very lucky to get a kind support from each and every member of the group and as well as getting an award for being "the least relaxed and the most quoted member of the group". My special thanks go to Dr R. C. Reed (role model in the early stage of my Ph.D), Dr S. A. Atamert, Dr S. A. Khan, Dr A. Ali (for valuable discussions on bainite and for excellent collection of references), Dr N. I. A. Haddad (for passing on the dilatometer to my hands), Dr M. Baloch, Dr P. Wilson, Mr M. Takahashi (for help with dilatometer), Mr Tan Lihe, Mr G. I. Rees (the great philosopher, for a very illuminating discussion on allotriomorphic ferrite), Mr S. A. Mujahid (whose patience could not be matched), Mr S. Sharafi, Mr. A. Matsuzaki and Mr H. Ullah. Finally I should thank Ms N. Deards, Ms J. M. Race and Ms R. Thompson for taking the time to proof read my reports and also for being the chief architects of bringing elegance to the PT group! I would also acknowledge the considerable help of Mr J. Leader, Mr B. Seymour, Mr D. Nicol, Mr D. Duke, Mr G. Morgan, Mr B. Barber and Mrs Carol Best in technical matters. Thanks are also due to my colleagues from Japan, who taught me how to play base ball and encouraged me to learn japanese.

I would acknowledge my friends in department and Cambridge, who supported me with love and care to go through each and every moment of my stay in Cambridge and also for thought provoking general discussions. Finally I would like to dedicate this dissertation to my mother, brothers and sisters without whose moral support, I would have never made it to this stage.

Contents

Chapter 1: Introduction

1.1 Fusion Welding	1
1.1.1 Welding	1
1.1.2 Welding Metallurgy	2
1.2 Austenite to Ferrite Transformation	3
1.2.1 Reconstructive Transformations	3
1.2.2 Displacive Transformations	3
1.2.3 Allotriomorphic ferrite formation	4
1.2.4 Widmanstätten ferrite formation	6
1.2.5 Bainite formation	7
1.2.6 Acicular ferrite formation	8
1.2.7 Martensite formation	9
1.3 Overall Model of Weld Microstructure	9
1.3.1 Weld Cooling Curve	9
1.3.2 Characteristic transformation temperatures	9
1.3.3 Prediction of TTT diagrams	10
1.3.4 Columnar austenite grain size	11
1.3.5 Microstructure Calculation Procedure	12
1.4 Chromium - Molybdenum Steel	14
1.5 Prediction of Microstructure in Fe-Cr-Mo-C Welds	15

Chapter 2: General Experimental Techniques

2.1 Alloys	26
2.2 Sample Preparation and Heat Treatments	27
2.3 Dilatometry	27
2.4 Lattice Parameters Measurement	28
2.5 Metallography	29
2.5.1 Transmission electron microscopy - EDX	29
2.5.2 Scanning electron microscopy - EDX	29
2.5.3 Light Microscopy and microhardness testing	29
2.6 Thermomechanical Simulator	30

Chapter 3: The Microstructure of Fe-Cr-C Weld Metals

3.1 Introduction	34
3.2 Analysis of Published Data	34
3.3 Experimentation	35
3.4 Results and Discussion	36
3.4.1 Austenite grain size variation with chromium content in weld	36
3.4.2 Microstructure	36

3.5 Summary	39
Chapter 4: The Transition from Bainite to Acicular Ferrite in Reheated Weld Deposits	
4.1 Introduction	55
4.2 Experimentation	56
4.2.1 Alloy	56
4.2.2 Furnace Heat Treatments	56
4.2.3 Dilatometry	58
4.2.4 Measurement of linear thermal expansion coefficients	59
4.2.5 Lattice Parameters	60
4.2.6 Microscopy	60
4.3 Results	60
4.3.1 Effect of allotriomorphic ferrite	60
4.3.2 Dilatometry	63
4.4 Discussion	65
4.4.1 Static case	66
4.4.2 Dynamic case	67
4.5 Conclusions	68
Appendix	69
Chapter 5: Mechanism of the Transition from Bainite to Acicular Ferrite	
5.1 Introduction	95
5.2 Method and Experimental Techniques	95
5.3 Results and Discussion	96
5.3.1 Heat-Treatment	96
5.3.2 Interpretation of Dilatometry Data	99
5.4 Conclusions	100
Chapter 6: Continuous Cooling Transformation Characteristics of Fe-Cr-C Reheated Weld Metals	
6.1 Introduction	112
6.2 Experimentation	113
6.2.1 Interpretation of Dilatometry Data	113
6.3 Results	114
6.4 Discussion	116
6.5 Conclusions	116
Chapter 7: A Direct Study of Grain Boundary Allotriomorphic Ferrite Crystallography	
7.1 Introduction	125

7.2 Experimental Methods	126
7.2.1 Alloys and Heat Treatment	126
7.2.2 Metallography	126
7.3 Crystallographic Technique	127
7.4 Results and Discussion	128
7.4.1 Allotriomorphic Ferrite/Austenite Orientation Relations	128
7.4.2 Ferrite Orientation with respect to both adjacent austenite grains	130
7.4.3 Bainite/Austenite Grain Boundary Crystallography	133
7.4.4 Detailed Examination of Particular Allotriomorph	134
7.4.5 Chemical Composition of Allotriomorphic Ferrite	134
7.5 Summary & Conclusions	136

Chapter 8: Stress and the Acicular Ferrite Transformation

8.1 Introduction	149
8.2 Experimental Method	150
8.2.1 The Applied Stress	151
8.3 Results and Discussion	152
8.3.1 The Microstructure	152
8.3.2 The Transformation Strains	153
8.4 Conclusions	154

Chapter 9: Effect of Cobalt on Fe-Cr-Mo-C Weld Deposits

9.1 Introduction	164
9.2 Design of Welds	164
9.3 Experimentation	165
9.4 Results and Discussion	166
9.5 Summary	167

Chapter 10: Future Research	175
---------------------------------------	-----

REFERENCES

ABSTRACT

This project is a part of the continuing research to predict the evolution of microstructure and properties in steel welds.

It has been suggested that an increase in the Cr and Mo concentration in steel welds should lead to a corresponding increase in the fraction of acicular ferrite, which is a desirable microstructure. In fact, the acicular ferrite volume fraction goes through a maximum as the Cr and Mo concentrations are increased. It is found that this unexpected effect can be attributed to a transition from acicular ferrite to bainite. Factors controlling the transition from acicular ferrite to bainite have been investigated. It appears that the presence of allotriomorphs of ferrite at the austenite grain boundaries has the effect of suppressing the formation of bainitic sheaves. This, in turn allows the acicular ferrite plates to develop on intragranular nucleation sites. A theoretical analysis indicates that the bainitic transformation is prevented from developing at the allotriomorphic ferrite/austenite boundaries by the carbon concentration profile present in the austenite at the allotriomorphic ferrite/austenite interface.

The crystallography of the grain boundary allotriomorphic ferrite has been studied with the aim of estimating the fraction of ferrite-austenite interfaces capable of developing into plates of Widmanstätten ferrite. The direct measurement of austenite orientation was made possible by using steels containing relatively large concentrations of silicon, heat treated in two stages to enable the retention of a substantial volume fraction of austenite at room temperature. The fraction of allotriomorphs exhibiting a reproducible orientation relationship with austenite is found to be rather small, as a consequence of the higher mobility of more incoherent $\alpha - \gamma$ boundaries. Allotriomorphs showing an orientation relationship with both the adjacent austenite grains are found to be very rare. The tendency for the allotriomorph to adopt an orientation which optimizes its fit with respect to both austenite grains with which it is in contact is also found to be small. Microanalysis data and their theoretical interpretation confirm that the transition from equilibrium to para-equilibrium growth can not be predicted by the usual method based on an estimation of the solute diffusion distance in the austenite.

For successful transition from bainite to acicular ferrite, the allotriomorphic ferrite has to be inert, *i.e.*, unable to develop into Widmanstätten ferrite or bainite sheaves. Detailed experiments are reported to verify that the allotriomorphic ferrite can be rendered inert by the build up of carbon in the austenite ahead of the allotriomorphic ferrite/austenite boundary. Controlled experiments, simulating the continuous cooling characteristics of welding, illustrated the importance of cooling conditions on acicular ferrite microstructure development. The temperature at which the maximum extent of transformation to acicular ferrite occurs is related to its plate size.

Acicular ferrite is considered to be identical in transformation mechanism to bainite, except that it nucleates intragranularly on inclusions, and hence develops into a morphologically different microstructure. The transformation causes displacements which, on a macroscopic scale, are characteristic of an invariant-plane strain with a large shear component. It is therefore expected that the transformation should be sensitive to an appropriate, externally applied stress. Results are presented which demonstrate quantitatively that large changes in the development of the microstructure are induced when acicular ferrite grows while the austenite is in compression. This is in spite of the fact that the applied stress used was below the austenite yield strength.

Cobalt (4.3 wt.%) was added to Fe-0.04C-2.25Cr-1Mo (wt.%) welds to stimulate the formation of allotriomorphic ferrite, and hence of acicular ferrite. No effect on allotriomorphic ferrite reaction kinetics was observed and hence no acicular ferrite formed in the welds. The reasons for this are unknown at this point and further work is needed.

Nomenclature and Abbreviations

a_γ^0	Lattice parameter of unalloyed austenite
\bar{a}_γ	Lattice parameter of alloyed austenite
\bar{a}_α	Lattice parameter of ferrite at ambient temperature
a_{Fe}^0	Lattice parameter of pure iron at ambient temperature
Ae_3	Upper limiting temperature of the $\alpha + \gamma$ phase field at equilibrium
Ae'_3	Upper limiting temperature of the $\alpha + \gamma$ phase field at paraequilibrium
Ae'_1	Lower limiting temperature of the $\alpha + \gamma$ phase field at paraequilibrium
AWS	American Welding Society
B_S	Bainitic transformation start temperature
C_i	Coefficient relating the effect of the concentration of element i on the lattice parameter of austenite
CCT	Continuous Cooling Transformation Diagram
\underline{D}	Weighted average diffusivity of carbon in austenite
e_c	Expansion in lattice parameter due to dissolved carbon
e_α	Linear thermal expansion coefficient of ferrite
e_γ	Linear thermal expansion coefficient of austenite
KS	Kurdjumov-Sachs orientation relationship
k_e	Equilibrium partition coefficient
k_p	Non-equilibrium partition coefficient
M_S	Martensitic transformation start temperature
$M_{Si, Mn, \dots}$	Mole fractions of alloying elements in the alloy
NW	Nishiyama-Wasserman orientation relationship
q	Half thickness of allotriomorphic ferrite
T_0	Temperature at which ferrite and austenite of identical composition have the same free energy
T'_0	Temperature at which ferrite and austenite of identical composition have the same free energy, taking into account the strain energy of the ferrite
T_i	Isothermal heat treatment temperature
T_C	Temperature at which the upper and lower 'C' curves of the TTT diagram intersect
T_α	Allotriomorphic ferrite transformation temperature
T_a	Intermediate annealing treatment temperature
T_b	Transformation temperature below B_s
T_h	Highest temperature at which allotriomorphic ferrite growth starts

T_l	Temperature at which allotriomorphic ferrite growth stops
TTT	Time-Temperature-Transformation
T_S	Temperature at which allotriomorphic ferrite formation begins during the cooling of austenite
T_1	First isothermal heat treatment temperature
T_2	Second isothermal heat treatment temperature
T_γ	Austenitising temperature
W_s	Widmanstätten ferrite transformation start temperature
\bar{x}_c	Average carbon concentration of the alloy
$x_c^{\alpha\gamma}$	Paraequilibrium α/γ interface carbon concentration in ferrite
$x_c^{\gamma\alpha}$	Paraequilibrium α/γ interface carbon concentration in austenite
x_{T_0}	Carbon concentration in austenite, as given by the T_0 curve
$x_{T'_0}$	Carbon concentration in austenite, as given by the T'_0 curve
V_a	Volume fraction of acicular ferrite
V_α	Volume fraction of allotriomorphic ferrite
V_W	Volume fraction of Widmanstätten ferrite
V_m	Volume fraction of microphases
α	Allotriomorphic ferrite
α_1	One dimensional parabolic thickening rate constant for paraequilibrium growth of ferrite
α_a	Acicular ferrite
α_b	Bainitic ferrite
α_W	Widmanstätten ferrite
γ	Austenite
δ	delta ferrite
ΔG_{max}	Maximum driving force for nucleation of ferrite from austenite
$\Delta G^{\gamma \rightarrow \alpha + \gamma'}$	Free energy change for austenite \rightarrow austenite + ferrite
$\Delta G^{\gamma \rightarrow \alpha}$	Free energy change for austenite \rightarrow ferrite with supersaturation
Δt_{850-T_i}	Time required to cool the sample from 850 °C to T_i , in seconds
τ_s	Time taken to establish a steady state nucleation rate

Chapter 1

Introduction

Modern manufacturing methods aim at optimising design and quality, hopefully without extra cost. This necessitates stringent selection of the manufacturing process variables for specific requirements, without much pre-production work. Models can help in predicting the response for the known set of variables.

Recently, Kirkaldy (1991) stressed the importance of modelling the thermomechanical behaviour of steels (Fig. 1.1). The approach is to predict the phase diagrams, kinetics of phase transformations and application of the same to transient heat and load conditions. Most of the manufacturing process like forging, rolling, casting and welding involve one or more of the variables mentioned in Fig. 1.1. The present research project pertains to the development of microstructure in steel welds. The theory discussed and developed can be of general use in the physical metallurgy of steels.

Welding has been applied in all critical fields like power plant, nuclear constructions, pipe lines, offshore structures and ship building. A fundamental understanding of the problems associated with welding has led to the development of welding procedures and specifications to a highly sophisticated level (Baker, 1975). These standard practices, mainly empirical codes, were developed by studying the properties of steel welds in conjunction with microstructure. In spite of this understanding and experience, pre-production approval tests are almost a standard requirement for any welded joint. This makes the selection of welding processes and variables itself, an expensive endeavour. A theoretical approach based on physical principles can therefore be beneficial.

The model developed by Bhadeshia *et al.*, (1985a) is a first step towards this approach; it successfully predicts the primary weld metal microstructure. The model also has been applied towards theoretical design of alloys for high strength weld metals, in a systematic new methodology. The present research project was initiated to explain certain anomalies observed in prediction of microstructure in Fe-Cr-Mo-C welds. The purpose here is to introduce welding terminology, aspects of steel welding metallurgy and chromium-molybdenum steels. The basis of the research described in the rest of this thesis, is presented at the end of this chapter.

1.1 Fusion Welding

Fusion welding is a permanent joining method, in which parts are joined together by melting.

1.1.1 Welding Processes

A widely used welding process is manual metal arc welding (MMAW or SMAW). An electric

arc is struck between a consumable metal rod, coated with mineral and metallic particles, and the joint as shown in Fig. 1.2. The movement of the electrode over the joint area is carried out by a qualified welder. This type of welding is the most flexible and versatile technique. Another common process is gas metal arc welding (GMAW or MIG), in which a continuously fed solid wire replaces the electrode of SMAW and the shielding is achieved by a flow of inert gas around the arc. In case of steel welding CO_2 gas is used. The productivity for GMAW is higher than SMAW. For thick plate structures, of the kind usually encountered in power plant steam headers and reactor vessels, submerged arc welding (SAW) or electroslag welding (ESW) is used. Both the processes use a molten slag as the main shielding medium to isolate the hot metal from the environment.

The properties of the weld depend on the microstructure, which relies on transient cooling conditions and restraints on the welds. Heat input given to the joint controls the cooling conditions. The heat input (Q) is determined by the welding voltage (V), the welding current (I) and the speed of welding (v_s), which is represented as:

$$Q = \frac{\eta VI}{v_s} \quad (1.1)$$

where η is the heat transfer efficiency (< 1.0), which depends on the welding process. Extensive work has been carried out to enable the prediction of the cooling conditions for a given weld geometry, using analytical equations, extensive numerical methods like finite difference and finite element methods (Rosenthal, 1941, Christensen *et al.*, 1965, Gray and Spence, 1982, Easterling, 1983).

1.1.2 Welding Metallurgy

There are two distinct regions of the joint which are of importance, namely, the weld metal (WM) and the heat affected zone (HAZ) as shown in Fig. 1.3.

Weld Metal:

This is the filled-in portion of the joint gap, which actually bonds the base-plates. The weld metal exhibits a columnar solidification microstructure similar to 'as cast' structures. The evolution of this columnar microstructure is often described as "epitaxial growth" (Easterling, 1983). The solidifying grain is a continuation of a base plate grain at the fusion boundary. The activation energy for solidification is thus zero. The reviews by Savage (1980) and Davies and Garland (1975) discuss the effect of welding variables on the weld metal solidification structure. The columnar grain size and shape can be changed by altering the weld pool shape. The inoculation of the weld pool, oscillation of the welding arc by mechanical or electromagnetic techniques, welding current and voltage modulation, ultrasonic vibration and forced surface nucleation all influence the solidification microstructure (Kou, 1987, Davies and Garland, 1975).

Heat Affected Zone:

The heat affected zone, is the region in the base plate whose microstructure is changed as the temperature rises during welding, but remains below the solidus temperature. Any microstructural change depends on the alloy and its starting condition. On moving from the fusion line towards the original base metal structure, distinct regions can be observed within the HAZ, depending upon the peak temperature (T_p) to which it is heated (Fig. 1.3). These include the coarse austenite grain region, heated to 1300–1100 °C, fine austenite grain regions (1100–900 °C), partially austenitised region (900–700 °C) and tempered region (500–700 °C) (Reed, 1990, Srinivasan, 1985). The temperature ranges are approximate and it should be stressed that the classification of regions using the equilibrium phase diagrams are not appropriate, instead kinetic considerations have to be considered. The heat affected zone, especially in the coarse austenite grain region, may transform to hard constituents like martensite, which can degrade the weldment properties by embrittlement. The main difference between the HAZ and weld metal lies in the austenite grain structure and the large inclusion content of the latter. Details of the differences in transformation behaviour are discussed later.

1.2 Austenite to Ferrite Transformation

A better understanding can be gained when all the decomposition reactions of austenite are viewed together. There is ample evidence that the different forms of ferrite can be categorised into those which are displacive and the others which involve a reconstructive transformation mechanism.

1.2.1 Reconstructive Transformations

Reconstructive transformation involves a change in crystal structure and with possible redistribution of solute contents between parent and product phase. In this mode, atoms make random thermally activated random jump across the transformation interface. All elements including solvent atoms (Fe) diffuse during transformation in a way which minimises the strain energy.

1.2.2 Displacive Transformations

During displacive transformations, the atoms move less than an interatomic distance and retain their relative relationships with their neighbours. The transformation process *per se* is equivalent to the deformation of the parent crystal lattice (austenite) to the product crystal lattice (ferrite), an invariant plane strain shape deformation with a large shear component. No iron or substitutional alloying element diffusion takes place.

The structural change during displacive and reconstructive transformations differ and is explained schematically in Fig. 1.4. The different ferrite products that occur in welds as variations

of these two mechanisms of transformations are as follows;

- Allotriomorphic ferrite
- Widmanstätten ferrite
- Bainite
- Acicular ferrite
- Martensite

The mechanisms of transformation for the above phases are grouped as shown in Fig. 1.5. The martensite and austenite, which usually form in welds as aggregates, are known as “microphases”. The volume fraction of these is often very low in the case of low alloy steel weld deposits. The microstructure classification listed above is slightly different from the one proposed by the Welding Institute (Pargeter, 1983). The terminology by the Welding Institute considers Widmanstätten ferrite and bainitic ferrite as a single constituent. Each phase is now discussed in detail.

1.2.3 Allotriomorphic ferrite formation:

The allotriomorphic ferrite, (often called proeutectoid ferrite, grain boundary ferrite or polygonal ferrite), is the first phase to transform from austenite, on cooling. The term “allotriomorphic” means that the phase is crystalline in internal structure, but not in outward form (Christian, 1975). The allotriomorphic ferrite invariably nucleates along γ/γ boundaries and grows by a reconstructive transformation mechanism. The growth is not restricted by austenite grain boundaries.

The kinetics of grain boundary allotriomorphs has been studied extensively by many researchers (see review by Bhadeshia, 1985). The growth of allotriomorphic ferrite in Fe-C steel involves the partitioning of carbon into austenite and in most cases is limited by the diffusion of carbon in the austenite ahead of the interface. The diffusion-controlled growth of ferrite in Fe-C-X (where X represents a substitutional solute) steels is complicated by the fact that both interstitial and substitutional diffusion occurs during transformation. The respective diffusion coefficients differ substantially. In addition to this, the assumption of local equilibrium at the interface leads to a variety of possible growth modes (Hillert, 1951 and Coates, 1973c). To match the interstitial and substitutional fluxes and arrive at a unique α/γ interface velocity is only possible by varying the concentration gradients. For example, in the Fe-C-Mn system, the transformation involves diffusion of manganese and carbon (partitioning of both C and Mn into austenite). This leads to concentration profiles ahead of the moving interface as shown schematically in Fig. 1.6a. The interface compositions are under the local equilibrium assumption related by a tie-line for Fe-C-Mn phase diagram at that temperature. The conservation of mass at planar interface moving with a interface velocity “ v ”, in the direction Z (normal to the

interface plane) requires that in the first approximation;

$$(x_c^{\gamma\alpha} - x_c^{\alpha\gamma})v = -D_{11} \nabla x_c \quad (1.2)$$

$$(x_{Mn}^{\gamma\alpha} - x_{Mn}^{\alpha\gamma})v = -D_{22} \nabla x_{Mn} \quad (1.3)$$

where x_c and x_{Mn} represent concentrations of C and Mn and the gradients (∇x_{Mn} , ∇x_c) are evaluated at the position of the interface. $x_{c,Mn}^{\gamma\alpha}$, $x_{c,Mn}^{\alpha\gamma}$ are the compositions of the austenite and ferrite at the interface. D_{11} and D_{22} represent the diffusivities of C and Mn, as $D_{11} \gg D_{22}$, these equations can not be in general be simultaneously satisfied, by a tie-line passing through \bar{x}_c and \bar{x}_{Mn} . However, one possibility is to by select a tie line such that $x_c^{\gamma\alpha} \simeq \bar{x}_c$ (see Fig. 1.6b), so that flux of carbon is reduced to a rate consistent with diffusion of Mn. Ferrite growing by this mechanism is said to grow by "Partitioning Local Equilibrium" (PLE) mechanism, with long range diffusion of Mn in γ .

An alternate choice of tie line would be to allow $x_{Mn}^{\alpha\gamma} \simeq \bar{x}_{Mn}$, in which case the Mn gradient is increased, thus allowing it keep pace with C, satisfying the mass conservation (see Fig. 1.6c). This mode of ferrite transformation is said to occur by a "Negligible Partitioning, Local Equilibrium" (NPLE) mechanism. Both the transformation mechanisms involve local equilibrium because the composition of the interface are determined by a tie line of the phase diagram.

Kinetic factors often prevent transformations from occurring under equilibrium conditions. An example case is a phase change which ^{is} so rapid that one or more of the components can not redistribute among the phases in the time scale of the experiment (Cahn, 1980). In steels the diffusivities of interstitial and substitutional alloying element are very different. It is then possible to imagine a condition where the substitutional alloying element diffusion is so sluggish during $\gamma \rightarrow \alpha$ transformation and substitutional alloying elements may not partition, even though carbon may be allowed to partition (Hillert, 1951, Rudberg, 1952 and Aaronson *et al.*, 1966b). This constrained equilibrium between α and γ , where both phases have same substitutional to iron atom ratio, and yet the carbon achieves its equilibrium with both phases, is called "Paraequilibrium". The interface compositions are then given by the tie line to paraequilibrium phase diagram.

Because of the high cooling rates involved, the growth of allotriomorphic ferrite in welds can be assumed to occur by paraequilibrium transformation in which case it is controlled by the diffusion of carbon in the austenite ahead of the interface. The half-thickness of an allotriomorph at an austenite grain boundary for a particular time at a transformation temperature is given by following equation for one-dimensional thickening.

$$q = \alpha_1 t^{0.5} \quad (1.4)$$

where

α_1 is the one dimensional parabolic thickening rate constant

t is the time after the initiation of growth.

q is the half thickness of ferrite

The parabolic thickening rate is derived by solving the equation:

$$2(\underline{D}/\pi)^{0.5} \frac{(x_c^{\gamma\alpha} - \bar{x}_c)}{(x_c^{\gamma\alpha} - x_c^{\alpha\gamma})} = \alpha_1 \exp \left\{ \frac{\alpha_1^2}{4\underline{D}} \right\} \operatorname{erfc} \left\{ \frac{\alpha_1}{2\underline{D}^{1/2}} \right\} \quad (1.5)$$

where

$x_c^{\gamma\alpha}$ is the paraequilibrium carbon in austenite,

$x_c^{\alpha\gamma}$ is the paraequilibrium carbon in ferrite,

\bar{x}_c is the average carbon concentration in the alloy,

\underline{D} is a weighted average diffusivity of carbon in austenite given by Trivedi and Pound (1967).

$$\underline{D} = \int_{x_c^{\alpha\gamma}}^{x_c} \frac{D\{X\} dx}{(\bar{x}_c - x_c^{\gamma\alpha})} \quad (1.6)$$

where $D\{X\}$ is calculated based on the method due to Siller and Mclellan (1969,1970) and Bhadeshia (1981b). The method takes into account the concentration dependence of the diffusivity of carbon in austenite. The calculation thus requires a knowledge of the phase diagram; the method for estimating such diagrams has been already developed by Bhadeshia and Edmonds (1980). The application of these ideas to continuous cooling conditions of ^{the} weld are presented in the next section.

1.2.4 Widmanstätten ferrite formation

Widmanstätten ferrite forms as thin wedge shape plates nucleated from austenite grain boundaries. It always has a KS/NW type crystallographic orientation relationship with the austenite. Secondary Widmanstätten ferrite develops from the grain boundary allotriomorphic ferrite. It is believed that Widmanstätten ferrite grows by a displacive mechanism because there is an invariant-plane strain (IPS) shape change accompanying its growth. The strain energy due to the shape change is reduced (to about 50 J mol⁻¹) by the coupled growth of mutually accommodating variants. The rate is, however, controlled by the diffusion of carbon in austenite. Widmanstätten ferrite can occur as packets of plates. The thickening of these plates will be stifled by the diffusion fields of nearby plates (often called "soft impingement"). The lengthening rate G of Widmanstätten ferrite can be estimated using Trivedi's (1970) theory for the diffusion

controlled growth of parabolic cylinders. Because of its shape, and unlike allotriomorphic ferrite, Widmanstätten ferrite grows at a constant rate as long as soft impingement does not occur.

1.2.5 Bainite formation:

Bainite is often found in the weld metals having high alloy contents and occurs as a non-lamellar mixture of ferrite with or without carbides. The ferrite is in the form of clusters of thin platelets, called sub-units. Bainitic transformation leads to an IPS shape change and occurs without substitutional alloying element partition^{ing}. The mechanism appears to be displacive (Bhadeshia and Edmonds, 1980). The sheaf grows by the repeated nucleation and growth of new sub-units. The initial nucleation event takes place at the prior austenite grain boundaries and subsequently, sub-units nucleate and grow from the tips of the previous sub-units (Christian and Edmonds, 1984, Bhadeshia and Christian, 1990).

The formation of bainitic ferrite leads to an increase in carbon concentration of the remaining austenite. It is believed that the bainitic ferrite sub-unit forms without any carbon compositional change, but after the transformation event carbon then diffuses rapidly into the austenite. There are two morphological bainitic ferrites observed in steel. Upper bainite is obtained if the time taken for the carbon diffusion process is small when compared with that required for the precipitation of carbides in the bainitic ferrite. Otherwise the transformation product is conventionally classified as lower bainite, with carbides being present inside the bainitic ferrite. The morphology of individual plates of bainite is determined by the need to minimise the strain energy owing to the IPS shape change associated with the displacive transformation. The bainitic transformation also exhibits characteristic IPS surface relief effect. The elastically accommodated strain energy is estimated to be around 400 J mole⁻¹.

Bainite forms below the T_0 temperature where the austenite and bainitic ferrite of the same chemical composition have equal free energy. This makes it thermodynamically possible for the transformation to be diffusionless. The diffusion of the carbon from the ferrite into the austenite constantly enriches austenite. The time scale of this process is of the order of fraction of a second. This makes it impossible to determine directly the concentration of carbon in the ferrite during its growth. There is, however, an indirect method of assessing the conditions that exist during transformation. If the carbon concentration of the austenite (x_γ) exceeds that given by the T_0 curve, the diffusionless transformation stops. It has been verified using many different experimental techniques (Bhadeshia and Christian, 1990) that the growth of bainitic ferrite stops at the phase boundary where $x_\gamma \simeq x_{T'_0}$. The T'_0 considers the strain energy of ferrite also (see Fig. 1.7).

The lengthening of bainitic platelets occurs at a rate much faster than would be expected from growth being controlled by diffusion of carbon in the austenite ahead of the interface.

Direct observation of the interface using the atom probe technique have demonstrated that substitutional solute atoms such as manganese, silicon, chromium, nickel and molybdenum do not partition between the phases during the bainitic transformation, nor do they segregate to the transformation interface (Bhadeshia and Waugh, 1982).

1.2.6 Acicular ferrite formation:

There has been extensive research in the field of acicular ferrite development in welds with reference to effects of alloy compositions, cooling rate and other welding variables and the effect of this microstructure on properties (see reviews by Abson and Pargeter, 1986, Farrar and Harrison, 1987 and Grong and Matlock, 1986 and Ricks *et al.*, 1981 & 1982). The acicular ferrite is believed to give an optimum strength and toughness due to its fine grains and also the interlocking nature, often referred to as a "basket weave structure" (Liu and Olson, 1986). It is generally recognised that acicular ferrite has, in three dimensions, the shape of thin lenticular plate. The aspect ratio in a random section is about 0.1. The plates also contain a high dislocation density (Yang and Bhadeshia, 1990). The reviews by Grong and Matlock (1986) and Abson and Pargeter (1986), highlighted the mechanism of acicular ferrite formation and its effect on properties. There appears to be a strong dependence of the transformation on intragranular (within austenite matrix) inclusions. Some of the similarities between bainite and acicular ferrite can be summarised as follows:

1. There is no substitutional solute partitioning during the growth of either bainite or acicular ferrite (Strangwood and Bhadeshia, 1987a).
2. Both reactions stop when the austenite carbon concentration reaches a value where it becomes thermodynamically impossible to achieve diffusionless growth (Yang and Bhadeshia, 1987a; Strangwood and Bhadeshia, 1987a).
3. Acicular ferrite only forms below the bainite-start temperature. (Ito *et al.*, 1982)
4. There is a large and predictable hysteresis in the temperature at which austenite formation begins from a mixed microstructure of acicular ferrite and austenite, or bainite and austenite (Yang and Bhadeshia, 1987b,c, 1989b).
5. The removal of inclusions from a weld deposit, without changing any other feature, causes a change in the microstructure from acicular ferrite to bainite (Harrison and Farrar, 1981).
6. An increase in the number density of austenite grain surface nucleation sites (relative to intragranular sites) causes a transition from acicular ferrite to bainite (Yang and Bhadeshia, 1987a).
7. Like upper and lower bainite, it is possible to obtain upper and lower acicular ferrite. Plates of lower acicular ferrite, like lower bainite, contain fine precipitates of cementite in a single orientation (Sugden and Bhadeshia, 1989b).

8. At free surfaces, both acicular ferrite and bainite cause displacements which are characterised as invariant-plane strains with large shear components. Consequently, the growth of a plate of acicular ferrite or bainite is confined to a single austenite grain (*i.e.*, it is hindered by a grain boundary) since the coordinated movement of atoms implied by the shape change cannot in general be sustained across a border between grains in different crystallographic orientations. A further implication is that plates of acicular ferrite, like bainite, *always* have an orientation relationship with the parent phase, which is within the Bain region.

1.2.7 Martensite formation:

Martensite is a product of diffusionless transformation. In welds, it forms in the small amount of residual austenite that remains after the higher temperature products have formed. The martensite in normal low alloy steel weld deposits occurs only in small quantities, mostly limited to the regions which are called microphases, which also contain some retained austenite. In certain high strength welds it is possible to have microstructures with large quantities of martensite but the carbon concentration must then be kept very small to avoid hydrogen cracking (Svensson and Bhadeshia, 1988).

1.3 Overall Model of Weld Microstructure

The microstructure evolution as a function of transformation temperature is shown schematically in Fig. 1.8. The flow chart describing the weld microstructure model is given in Fig. 1.9.

1.3.1 Weld Cooling Curve

The nature of heat flow in welding is two dimensional or three dimensional (or indeed an in between case). At temperatures, below melting point of the fusion zone, the cooling rate is virtually independent of the position (AWS, 1981). An equation of the form

$$dT/dt = (C_1/Q)(T - T_i)^{C_2} \quad (1.7)$$

can then be used empirically to represent the weld metal cooling rate, with C_1, C_2 taken to be adjustable constants obtained by fitting the experimental data (Svensson *et al.*, 1986). T_i is the interpass temperature, T is temperature of interest and Q is the heat input given to the weld (see equation 1.1).

1.3.2 Characteristic transformation temperatures

The transformation temperatures are calculated using free energy change for transformation from austenite to ferrite. The free energy calculations are based on a method published

elsewhere (Shiflet *et al.*, 1978, Aaronson *et al.*, 1966a& b and Bhadeshia, 1980a, 1982a). Initiation of Widmanstätten ferrite and bainite necessitates a minimum driving force for nucleation (ΔG_{max}) given by a universal G_N function. The G_N function was derived by fitting ΔG_{max} with the published transformation temperature data of Steven and Haynes (1956). Another function which was based on $\Delta G^{\gamma \rightarrow \gamma' + \alpha}$ was also derived. It was found that similar results were obtained by use of either one of the functions. The use of ΔG_{max} for nucleation of displacive products may suggest that the nucleation may involve partitioning of carbon, during displacive transformation to Widmanstätten ferrite and bainite. And this may not be operative in the growth stage. The transformation temperatures should consider the growth conditions. Thus the following conditions are applicable for transformation start temperatures of Widmanstätten ferrite and bainite.

$$\left. \begin{array}{l} \Delta G_{max} \geq G_N \\ \Delta G^{\gamma \rightarrow \alpha + \gamma'} \geq 50 \text{ J mole}^{-1} \end{array} \right\} \text{ for Widmanstätten ferrite} \quad (1.8)$$

Here the 50 J mole⁻¹ is needed to satisfy the stored elastic transformation strain energy during transformation.

$$\left. \begin{array}{l} \Delta G_{max} \geq G_N \\ \Delta G^{\gamma \rightarrow \alpha} \geq 400 \text{ J mole}^{-1} \end{array} \right\} \text{ for Bainitic ferrite} \quad (1.9)$$

Here 400 J mole⁻¹ is needed to satisfy the stored elastic strain energy during bainitic transformation (Bhadeshia, 1981a).

For ^{the} martensitic start temperature a minimum free energy change has to be met by $\Delta G^{\gamma \rightarrow \alpha}$ for a given temperature (Bhadeshia, 1981c&d). The minimum free energy change has been given by ^{the} following equation.

$$\Delta G\{M_s\}_{minimum} = -1120.00 - f\{\bar{x}_c\} \text{ J mole}^{-1} \quad (1.10)$$

$$f\{\bar{x}_c\} = 10568.0\bar{x}_c + 94.1 \quad (1.11)$$

where \bar{x}_c is the mean carbon concentration in mole fraction.

1.3.3 Prediction of TTT diagrams

The methodology for this was developed by Bhadeshia (1982a). The time-temperature-transformation diagram is represented as two "C" curves, in which one represents reconstructive and the another displacive transformation. Given a chemical free energy change for nucleation (ΔG_{max}) of ferrite, the incubation time to achieve a detectable degree of transformation can be estimated. The equation for predicting the transformation time is after Russell's (1969) expression. The final form is as follows;

$$\tau \propto \frac{T}{(\Delta G_{max}^v)^p D} \quad (1.12)$$

where p is constant and $\Delta G_{max}^v = \Delta G_{max}/V^m$, where V^m , is the molar volume of ferrite. D is a diffusion coefficient related to boundary or volume diffusion, depending upon the state of the coherency of the nucleus. This can be represented by an activation energy term as given below.

$$D = D_0 \exp\{-Q/RT\} \quad (1.13)$$

T is the temperature in Kelvin and p an exponent whose magnitude is a function of the nature of the nucleus (Russell obtained a value of 2 for coherent nucleus and 3 for an incoherent state). In line with Bhadeshia (1982a), by substituting an expression for the term D , the final form of equation is as following:

$$\tau = T^a (\Delta G_{max})^b \exp\{c/T\}.d \quad (1.14)$$

where a, b, c & d were found by fitting the equation to published experimental data. Data were taken from BISRA (1956) atlas of isothermal transformation diagrams. This approach considers the effect of alloying elements through a modification in the value of ΔG_{max} . Thus, the calculation procedures can be extended to the unknown situations, as long as the effect of alloying addition on free energy modification is known. Note that there is no accounting for the austenite grain size, but as pointed out by Bhadeshia (1982a) this is reasonable for the very early stages of transformation.

1.3.4 Columnar austenite grain size

In the model developed for the prediction of the primary weld metal microstructure for Fe-Mn-Si-C weld deposits by Bhadeshia *et al.*, (1985) and modified by the work of Svensson *et al.*, (1986), the columnar austenite grain size has to be measured or calculated using an empirical correlation based on the heat input to the (Q , see equation 1.1) weld and the compositions in wt.%. The equation can calculate the mean linear intercept (on a transverse section in an orientation normal to the major axes of the columnar grains, \bar{L}_{tn}) of the prior austenite grain size for any heat input (Q) and also weld metal composition (only for manganese, silicon and carbon):

$$\bar{L}_{tn}(\mu m) = 64.5 - 445.8(\text{wt.\%C}) + 138.6(\text{wt.\%Si}) - 7.581(\text{wt.\%Mn}) + 16(Q, \text{kJ mm}^{-1}) \quad (1.15)$$

The mean linear intercept was then used to calculate the side length (a) of the hexagonal prism, which represents a columnar austenite grain in the microstructure model. The relation between \bar{L}_{tn} and the side length of a hexagonal cross section is given by:

$$\bar{L}_{tn}(\mu m) = \pi a \cos\{30^\circ\}/2 \quad (1.16)$$

The above relation (1.15) is empirical in nature. The equation was derived by multiple regression of the grain size, composition and heat input data. It is not yet possible to predict the austenite grain size from fundamental principles; even the factors controlling it are far from clear (Bhadeshia, 1989). For example, during solidification, those grains with their $\langle 100 \rangle$ directions most parallel to the direction of steepest temperature gradient grow rapidly, stifling the grains which are not suitably oriented. Consequently, the crystallographic texture of the parent plate, and the plane of that plate on which the weld is deposited, must influence the final austenite grain structure. Clear differences in the austenite grain structure were found between three welds deposited on mutually perpendicular faces of the same sample (Babu *et al.*, 1991).

1.3.5 Microstructure Calculation Procedure

After the calculation of weld cooling characteristics, austenite grain size, TTT diagrams, characteristic transformation temperatures and the paraequilibrium phase boundaries of a particular alloy composition, the overall calculation of microstructure can begin (Fig. 1.9). The transformation to allotriomorphic ferrite starts first (Fig. 1.8). Using the TTT data and the additive reaction rule (equation 59.9 of Christian, 1975), the temperature at which allotriomorphic ferrite begins (T_s) can be predicted. The model assumes that the austenite grain boundaries are uniformly covered by allotriomorphic ferrite, the instant ^{the} weld cools to T_s . The allotriomorphic ferrite then is assumed to grow, as the weld cools from T_s to a temperature T_C , the temperature at which the reconstructive 'C' and displacive 'C' curves of TTT diagram intersect as illustrated in Fig. 1.10. To allow for continuous cooling, ^{the} earlier isothermal growth equation (1.4) was differentiated with respect to time and assuming the variation of parabolic thickening rate to be negligible;

$$dq = 0.5\alpha_1 t^{-0.5} dt \quad (1.17)$$

Now integrating the above equation with respect to the total time spent on allotriomorphic ferrite reaction say t_1 (time taken to cool from T_s to T_C).

$$q = \int_{t=0}^{t_1} 0.5\alpha_1 t^{-0.5} dt \quad (1.18)$$

Once the thickness is found, assuming a hexagonal prism for the shape of the austenite grain and for a given austenite grain size, the volume fraction of allotriomorphic ferrite can be calculated using principles of stereology (Underwood, 1970).

$$v_{\alpha} = 2q \tan\{30^{\circ}\}(2a - 2q \tan\{30^{\circ}\})/a^2 \quad (1.19)$$

where a is the hexagon side length of the austenite grain and q is the half thickness of the allotriomorphic ferrite. The calculated volume fraction (v_{α}), after an empirical correction (V_{α}) as given below, was found to match very well with experimental data.

$$V_{\alpha} = 2.04v_{\alpha} + 0.035 \quad (1.20)$$

As soon as the temperature T_C is reached, the reconstructive transformation gives way to displacive transformation products. To start with, Widmanstätten ferrite emanates from the grain boundary allotriomorphic ferrite. It is important to note that the shape of Widmanstätten ferrite is such that the plate tip always advances into fresh austenite, so that it grows at a constant rate. The lengthening rate of Widmanstätten ferrite is found to be so high that the Widmanstätten ferrite can grow right across the austenite grain size in a fraction of second. The reaction can therefore be regarded as isothermal at T_C . The volume fraction of Widmanstätten ferrite is calculated by considering the shape to be a triangular prism and given by;

$$V_w = C_4 G(2a - 4q \tan\{30^{\circ}\})t_2^2/(2a)^2$$

G is the growth rate of Widmanstätten ferrite calculated at the temperature T_C , C_4 is a constant which is independent of the alloy composition and t_2 is the time *available* for the growth of Widmanstätten ferrite. Widmanstätten ferrite nucleates from allotriomorphic ferrite from a side which exhibits ^arational orientation relation (KS/NW) with austenite. Hence only certain proportion of available α/γ boundary area can be expected to develop into Widmanstätten ferrite. The constant C_4 thus incorporates the proportion of α/γ boundary capable of nucleating Widmanstätten ferrite. The consideration of physical impingement with acicular ferrite gave a good agreement with experimental data. The impingement with acicular ferrite is taken *into* account by comparing with time interval, represented by t_c , for the cessation of allotriomorphic ferrite growth and initiation of acicular ferrite reaction.

The amount of microphases (V_m) is calculated from ^{the} knowledge of paraequilibrium phase diagram. By assum^{ption} in welds, the transformation to allotriomorphic ferrite, Widmanstätten ferrite, and acicular ferrite occur to the maximum extent and by application of lever rule to Ae_1 and Ae'_3 lines at M_s temperature. The volume fraction of acicular ferrite is calculated by difference;

$$V_a = 1 - V_\alpha - V_W - V_m \quad (1.21)$$

where V_a is the volume fraction of acicular ferrite, V_α is the volume fraction of allotriomorphic ferrite, V_W is the volume fraction of Widmanstätten ferrite, V_m is the volume fraction of microphases.

It can be noted from the above equation that the maximum extent of transformation to acicular ferrite can be obtained by forcing V_α, V_W to a very small value. In high alloy welds it leads to a mixture of acicular ferrite / bainite and martensite. Thus, it is important to model the kinetics of bainite / acicular ferrite in those circumstances (Rees, 1990). The calculation of the relative amount of various phases, has been extended by Sugden and Bhadeshia (1988a), for the prediction of the properties of the primary weld metal microstructure. The calculation is based on factorising the strength of weld metal due to various factors. The factors are; namely strength of pure annealed iron, solid solution hardening and contribution from different microstructural morphologies like acicular ferrite, allotriomorphic ferrite and Widmanstätten ferrite. The weld model has shown considerable reliability for welds of most of the low alloy systems. The present research project was initiated on application of the model to Fe-Cr-Mo-C steel welds.

1.4 Chromium - Molybdenum Steels

Chromium - molybdenum steels have been used in petroleum industry reactor vessels, mainly to reduce corrosion by sulphur and its compounds which are present in crude oil. Their improved oxidation resistance and high temperature strength extended their application to other areas, like steam generators and heaters. Recently, they have also been used in hydro-treating vessels in the petroleum industry, where they are exposed to high temperatures and also high pressures of hydrogen. The service temperature is between 400 °C to 570 °C (Lundin *et al.*, 1986, AWS Vol. 4). The steels are used in two states, namely in the quenched and tempered condition but mostly in the normalised air cooled condition. The most widely used Cr - Mo steel is the so called 2.25Cr-1Mo wt.%. The microstructure is usually a mixture of allotriomorphic ferrite and bainite or completely bainite, with some retained austenite (Kar and Todd, 1982).

Cr - Mo steels can be welded by most welding processes, the choice being related to section thickness. To avoid embrittlement due to hydrogen, preheat or high heat input or the use of low hydrogen electrodes is suggested. For thin sections, preheat can be avoided. The filler metals used are of the same composition or slightly richer than that of the base metal. In case of using high chromium filler wires for the weld metal, for certain dissimilar composition joints, care should be taken not to expose the joints to very high temperatures. Such exposure to high

temperature ($>500\text{ }^{\circ}\text{C}$) will enhance carbon migration from the low Cr region to the high Cr region. This produces a soft region near the heat affected zone of the weldments. The welds are usually post weld heat treated depending upon alloy content and section thickness. For example the weld metal consisting of low carbon ($\approx 0.05\text{ wt.}\%$) need not be post weld heat treated (AWS, Vol. 4, 1972). The important properties of Cr - Mo steels and its welds to be considered are;

- creep strength,
- toughness,
- temper embrittlement resistance,
- hydrogen attack resistance,
- stress relief cracking resistance

The creep strength of these alloys depends mainly on the type and amount of carbide precipitate and its stability. It is found to be that the formation of coherent acicular Mo_2C carbides gives better creep properties with the ferrite microstructure grain size playing only a secondary role (Lundin *et al.*, 1986). Nevertheless, the toughness depends upon the ferrite microstructural features. Thus optimum combination of creep strength and toughness is an important parameter to be considered for Cr - Mo steels, and consequently microstructural development is worth studying.

1.5 Prediction of Microstructure in Fe-Cr-Mo-C Welds

Evans (1986,1988) published results of microstructure in weld metals containing chromium ($> 1.5\text{ wt.}\%$) and molybdenum ($> 0.5\text{ wt.}\%$). The weld microstructure model predicted continued increase of acicular ferrite as a function of alloy concentration. In contradiction, in real welds the columnar austenite grains of steel transform into bainite instead of acicular ferrite. This is in spite of the presence of non-metallic inclusions, which serve to intragranularly nucleate the plates of acicular ferrite. This has been also reported by Lundin *et al.*, (1986), McGrath *et al.*, (1989) and Josefsson *et al.*, (1987, 1989). The anomaly is explained schematically in Fig. 1.11.

It has been observed in the case of C - Mn steel welds that the optimum strength and toughness is obtained by maximising the acicular ferrite microstructure in the weld metal (Ito *et al.*, 1982). It is also known that the bainitic microstructure is poor in toughness compared with that of acicular ferrite. Thus a reintroduction of acicular ferrite in these welds could lead to a substantial improvement in properties. Hence, the present research programme concentrated on a fundamental understanding of acicular ferrite and bainite transformation behaviour in these steel welds, as presented in Fig. 1.12.

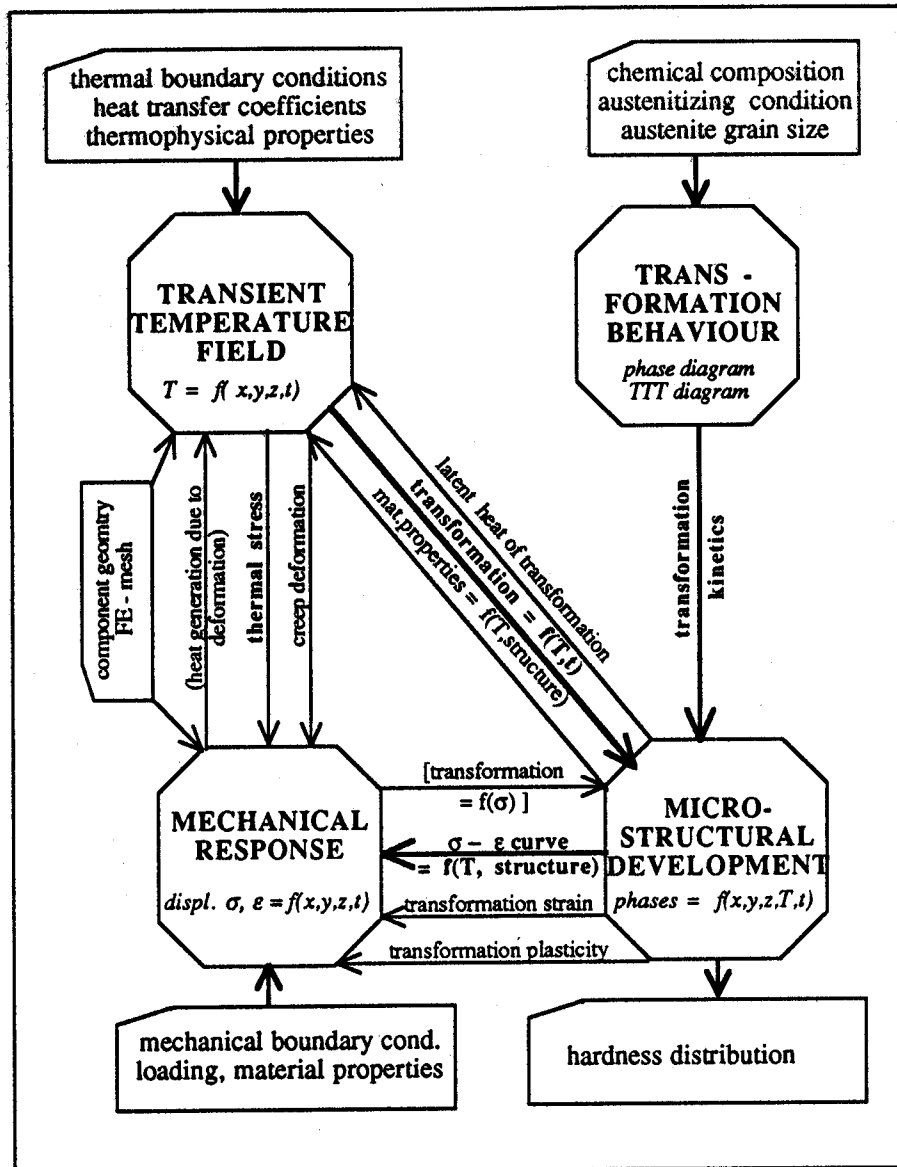


Fig. 1.1 Modelling phase transformations in steels, in response to thermomechanical conditions (after Kirkaldy, 1991).

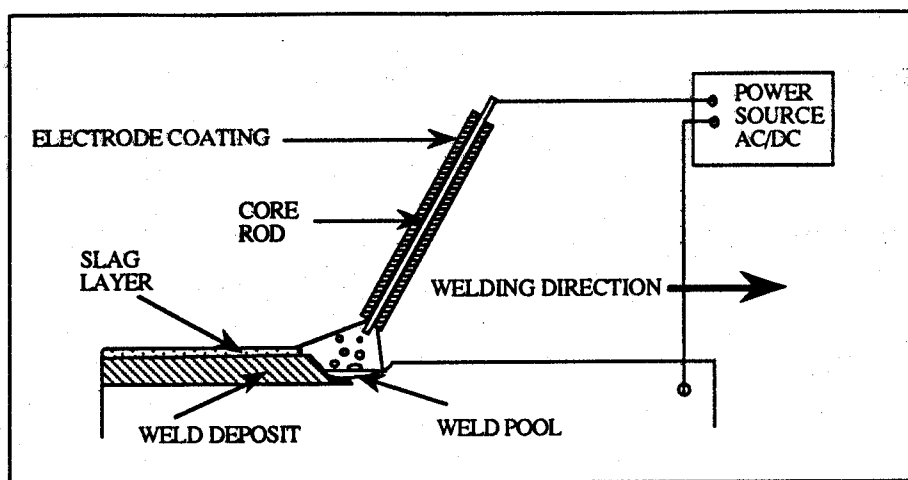


Fig. 1.2 The manual metal arc welding process (Gray and Spence, 1982).

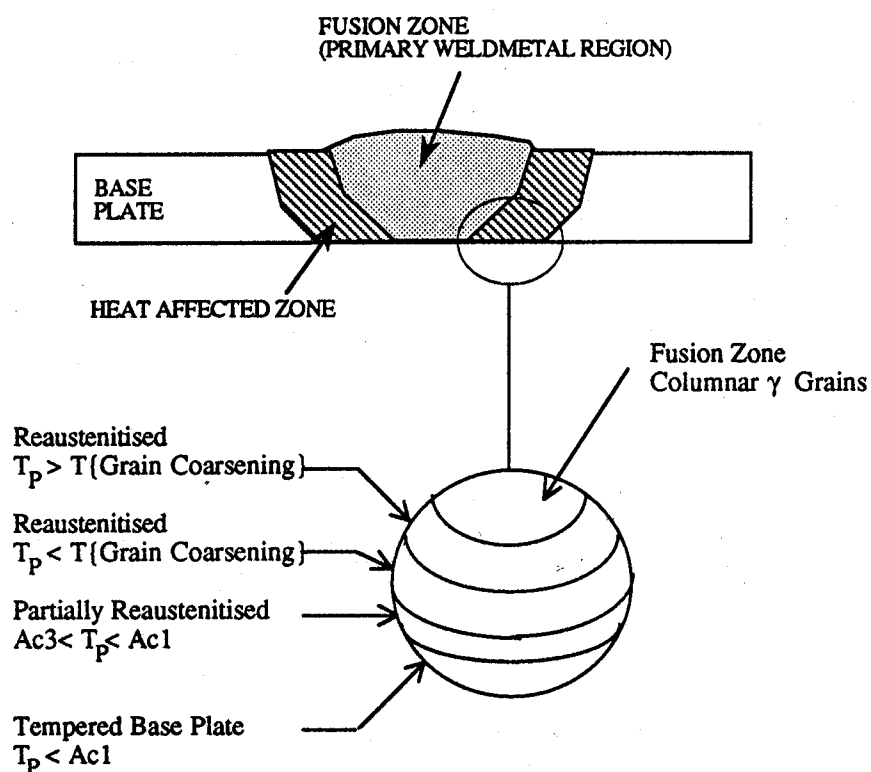


Fig. 1.3 The variety of regions of a typical weldment. T_p is the peak temperature experienced by a particular region. $Ac1$ and $Ac3$ are the dynamic transformation start and finish temperature from ferrite to austenite respectively.

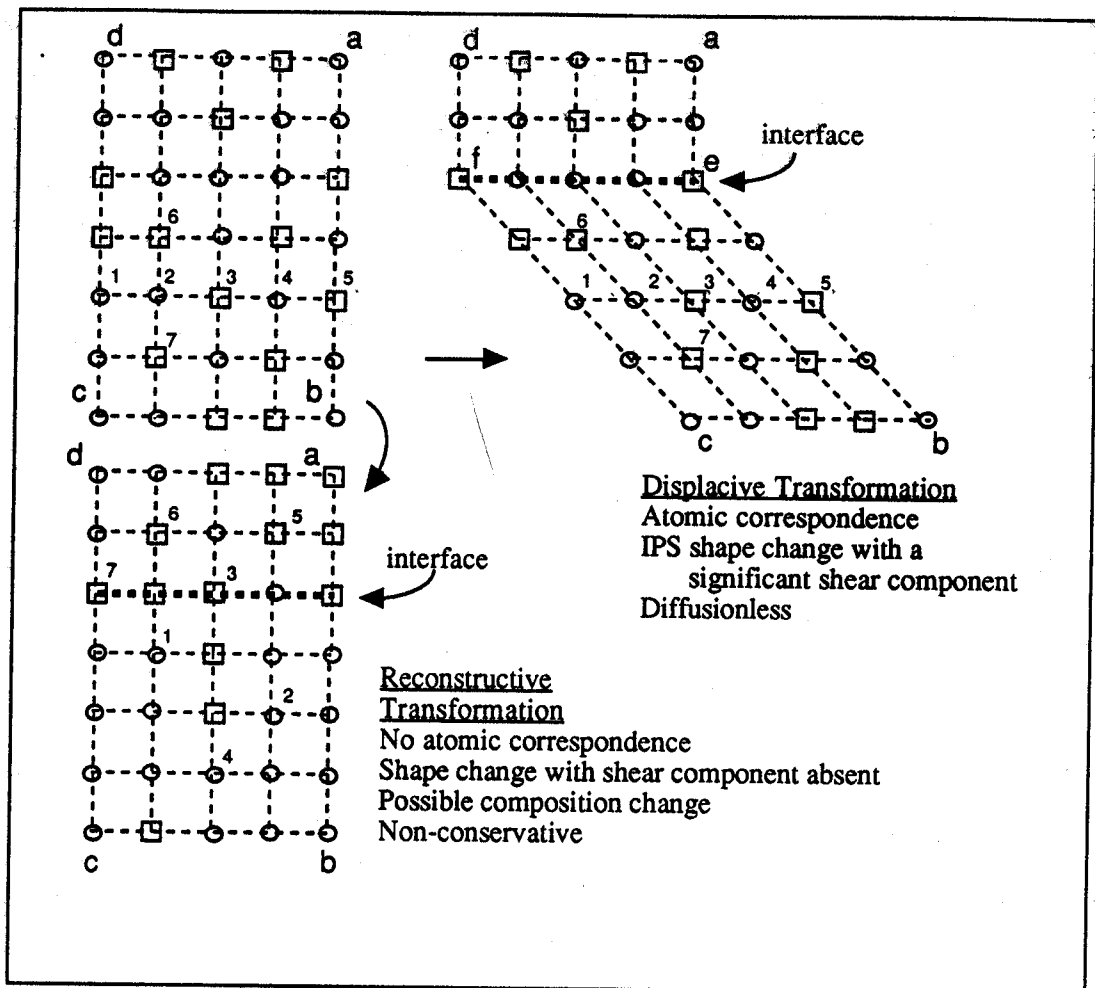


Fig. 1.4 Schematic illustration of the mechanisms of reconstructive and displacive transformations. The lines connect corresponding directions (Bhadeshia, 1987b).

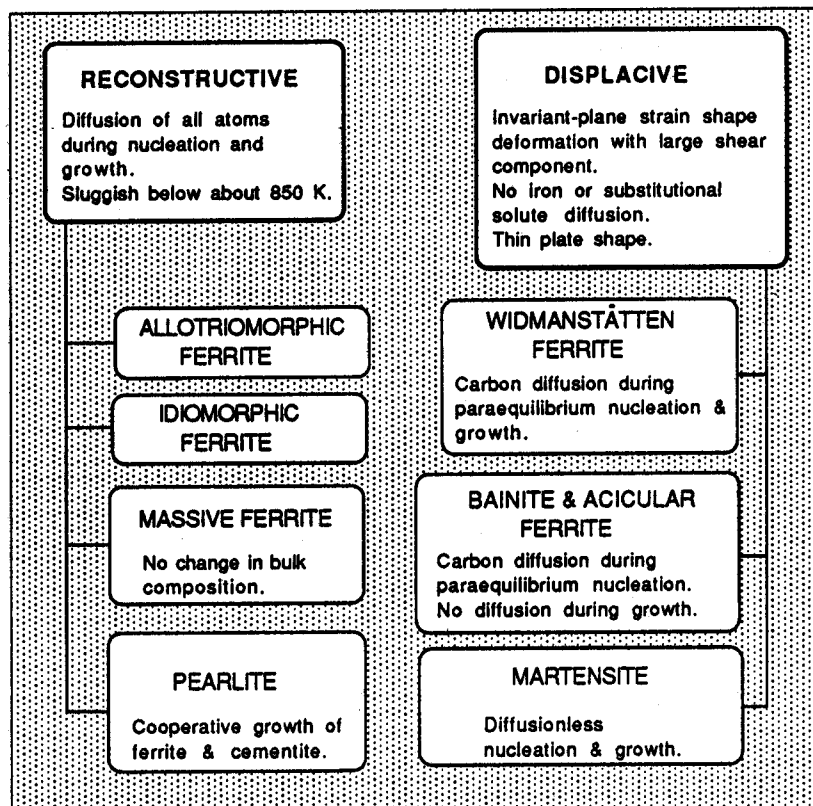


Fig. 1.5 Classification of various austenite to ferrite transformation products in steels based on transformation mechanisms.

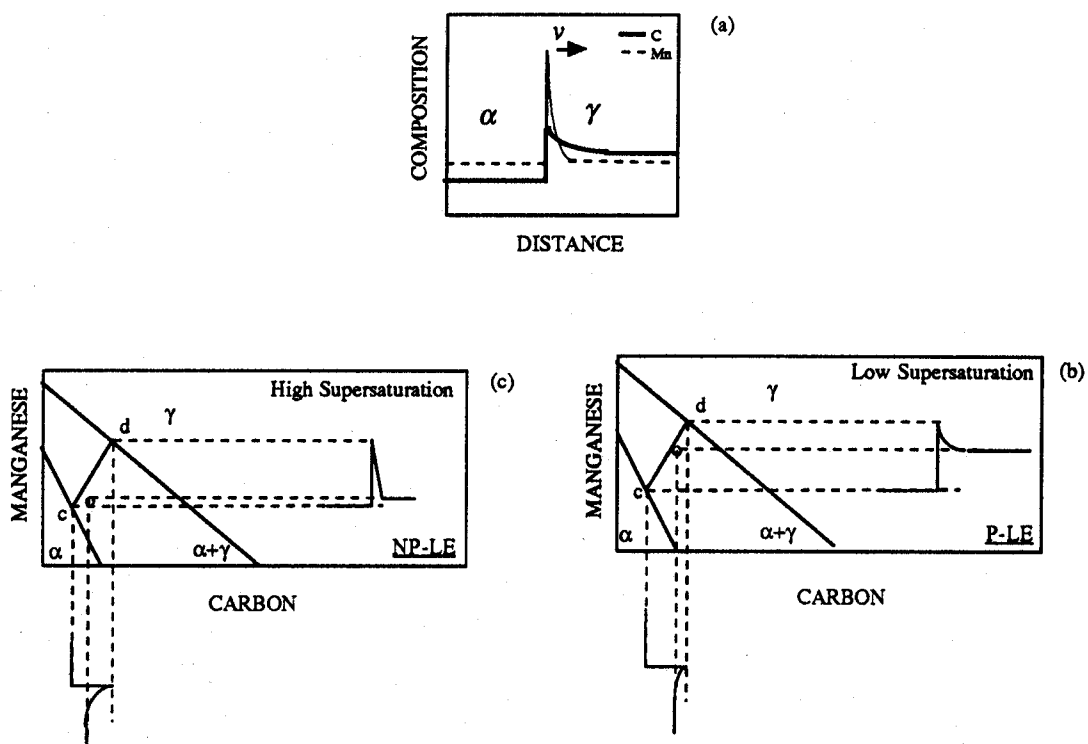


Fig. 1.6 Illustration of the transformation conditions to allotriomorphic ferrite growth, in a Fe-Mn-C system, with local equilibrium at the interface. (a) Schematic illustration of composition profile ahead of the moving α/γ interface. (b) Partitioning local equilibrium mode (PLE), (c) Negligible partitioning local equilibrium (NP-LE). The line cd in all cases defines a tie-line whereas the point o represents the alloy composition namely \bar{x}_c and \bar{x}_{Mn} .

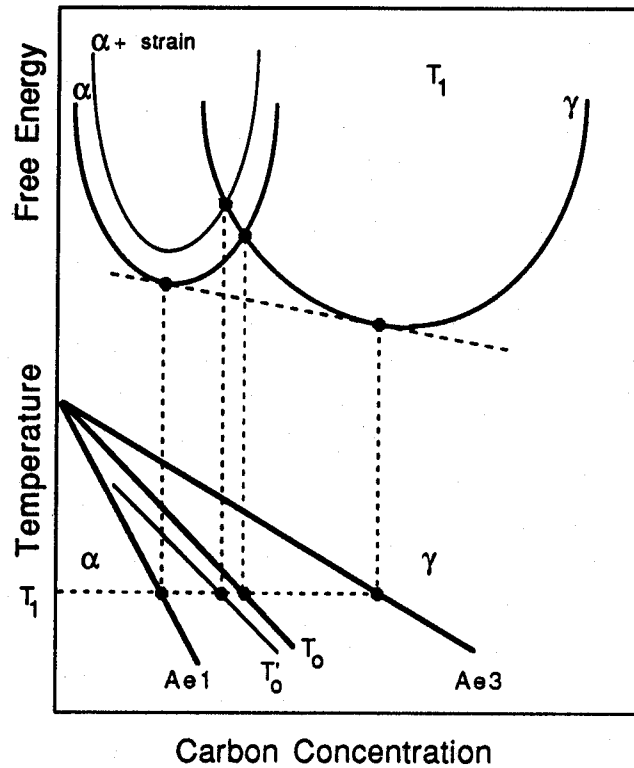


Fig. 1.7 Illustration of the incomplete reaction with paraequilibrium phase diagram and a free energy *vs* composition diagram. The carbon composition of residual austenite increases, as the transformation to bainite proceeds. The T'_0 phase boundary also considers the strain energy of ferrite (in case of bainite it is 400 J mole^{-1}).

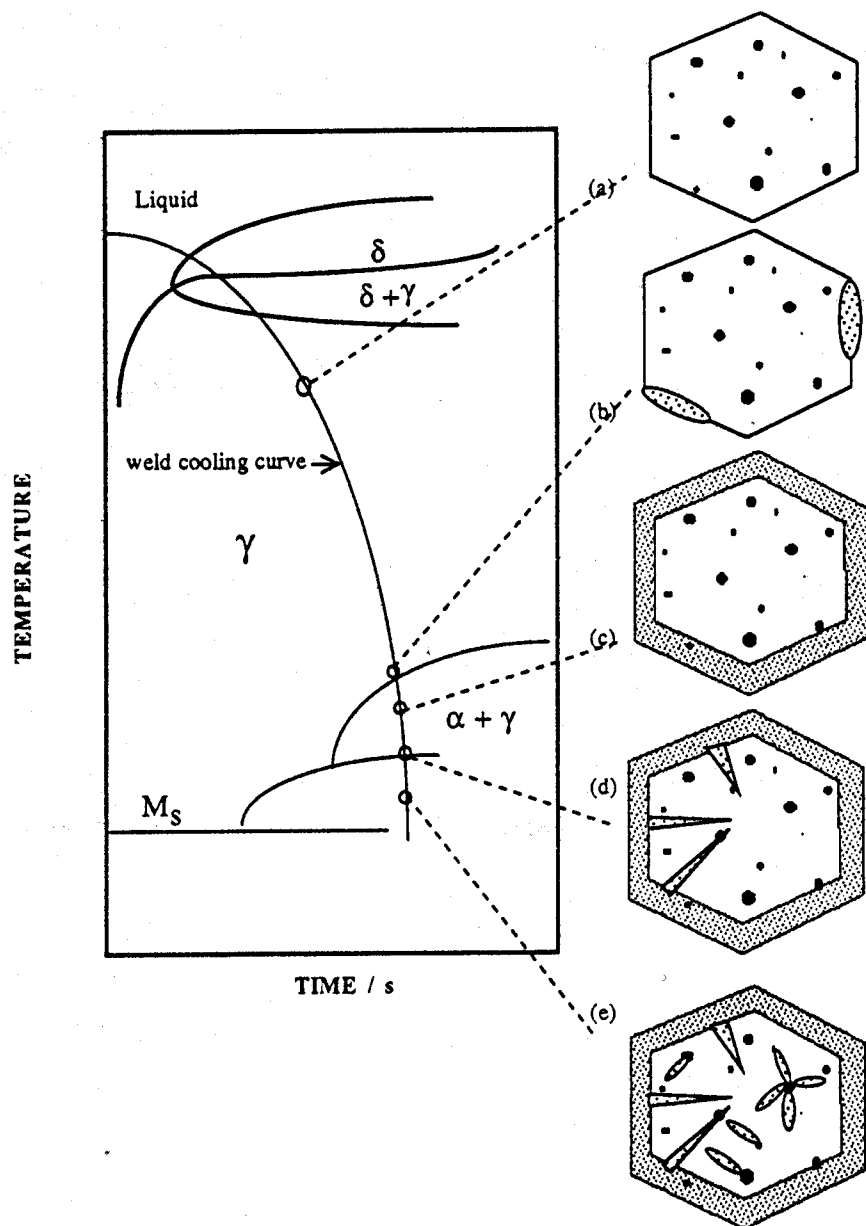


Fig. 1.8 Transformation sequences explained with the help of a schematic CCT diagram for a steel weld. The microstructure transformation sequence as a function of temperature being (a) austenite with oxide inclusions, (b) allotriomorphic ferrite nucleation, (c) site saturation of allotriomorphic ferrite and growth into austenite grain, (d) nucleation and growth of Widmanstätten ferrite, (e) nucleation and growth of acicular ferrite on inclusions and finally rest of the austenite transforms into martensite.

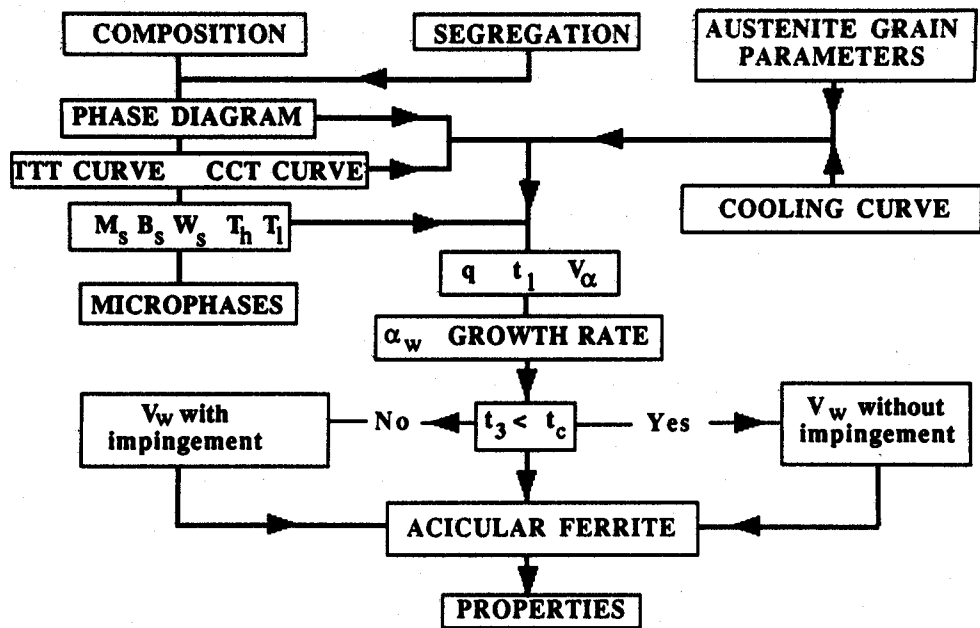


Fig. 1.9 Flow chart for overall weld microstructure prediction model (after Bhadeshia *et al.*, 1985).

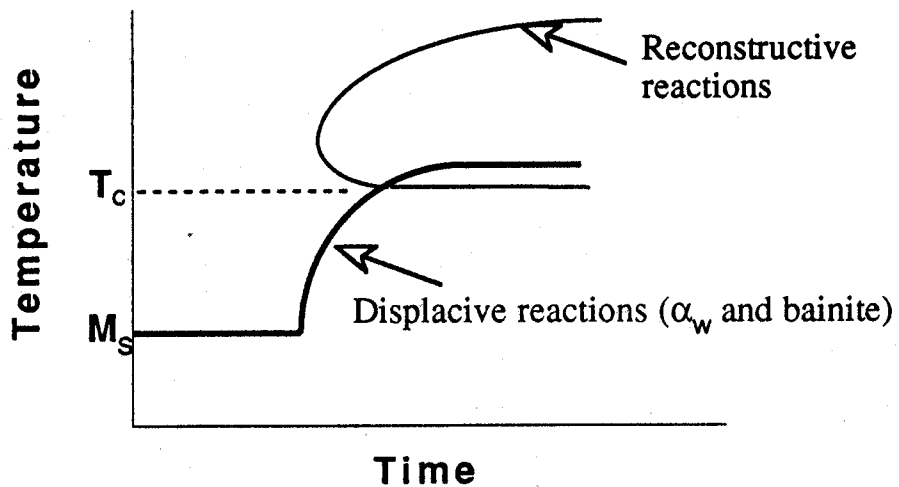


Fig. 1.10 Schematic illustration of TTT diagrams, and the temperature at which the reconstructive transformation give way to displacive transformation products (after Bhadeshia *et al.*, 1985).

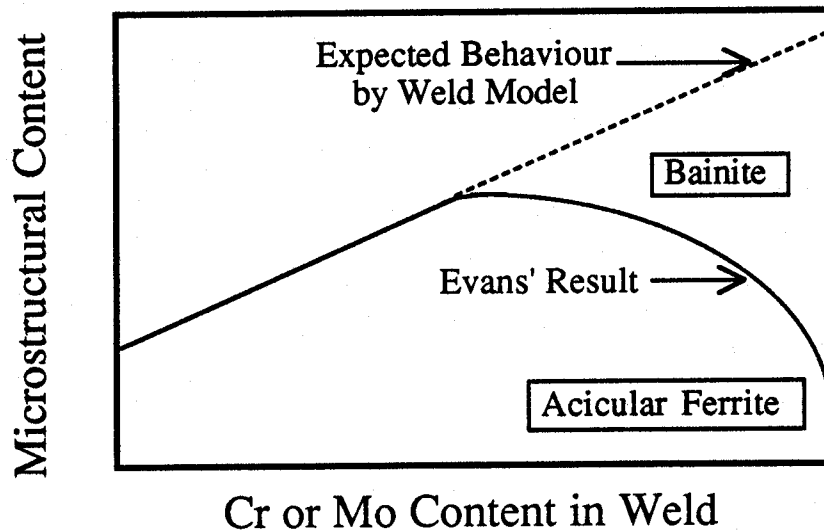


Fig. 1.11 Schematic illustration of the discrepancy observed in predicted volume fraction of acicular ferrite as a function of solute concentration with published results of Evans (1986 & 1988). Acicular ferrite was replaced by bainite after a certain degree of alloying.

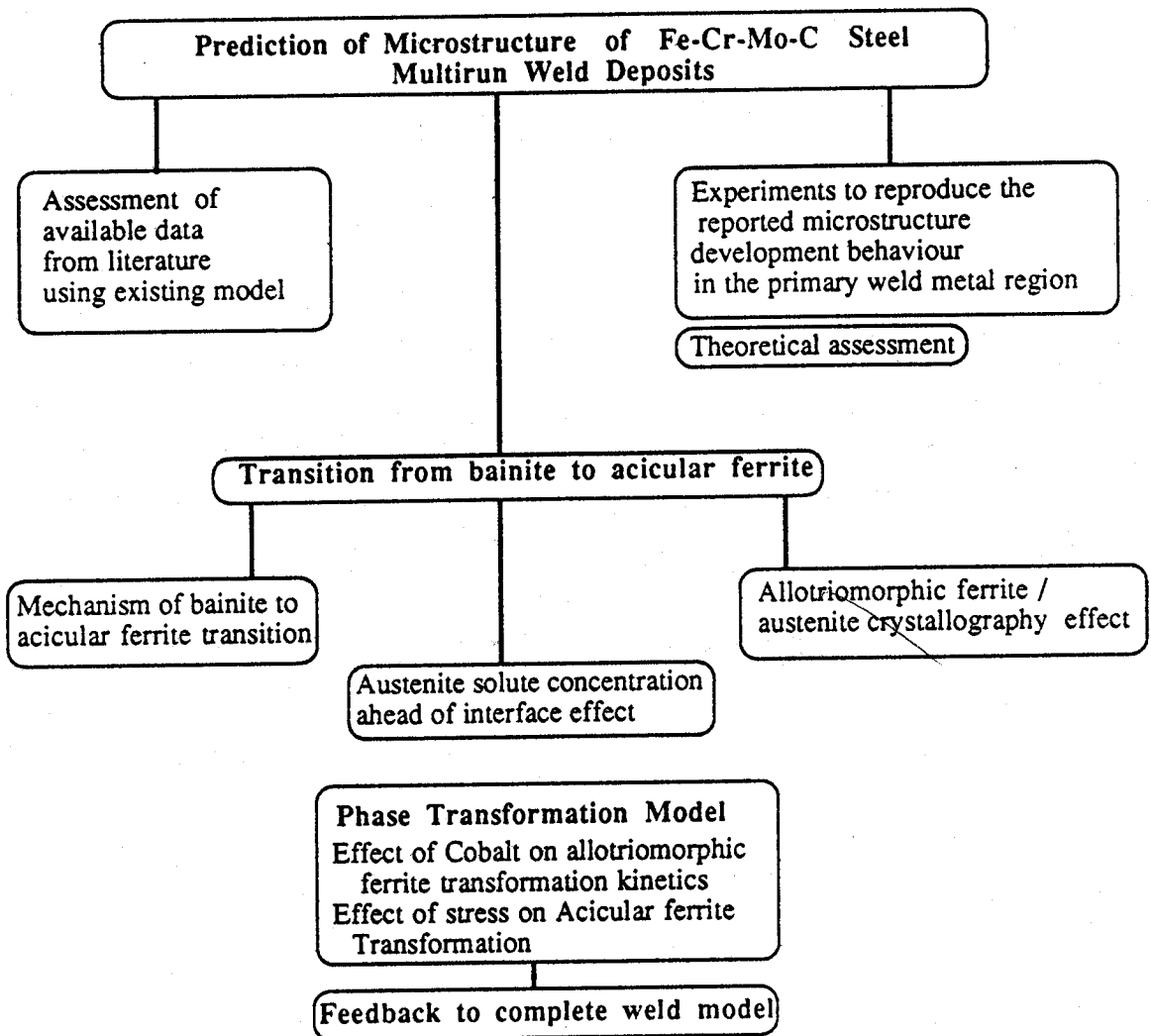


Fig. 1.12 Overview of the present research programme.

Chapter 2

General Experimental Techniques

2.1 Alloys

The alloys used were mainly weld metals. The samples were machined from all weld metal test pieces. The weld itself was fabricated according to the international standard ISO2560 (Fig. 2.1), The weld geometry is compatible with the minimisation of dilution effects associated with the melting of the base plate. The weld metal was deposited using the manual metal arc welding technique. The parameters used are listed in Table 2.1 and the chemical composition in Table 2.2.

Table 2.1 Welding process parameters.

Welding voltage	23 Volts
Welding current	120 Amps
Welding speed	0.004 m s ⁻¹
Interpass temperature	250 °C

Table 2.2 Weld metal composition in wt.%, with the oxygen and nitrogen concentration being stated in parts per million by weight.

ALLOY	C	Si	Mn	Ni	Mo	Cr	O _(ppm)	N _(ppm)
80	0.061	0.51	1.11	0.03	0.01	0.48	377	88
79	0.057	0.52	1.17	0.03	0.01	1.04	359	96
78	0.053	0.51	1.11	0.03	0.01	1.59	366	118
77	0.10	0.68	1.24	0.04	0.01	1.87	274	168
A1	0.04	0.39	0.91	0.04	1.13	2.51	503	89
AM1†	0.03	0.35	0.67	0.07	1.07	2.34	449	146

†also contains 4.3 wt.% cobalt

2.2 Sample Preparation and Heat Treatments

The samples machined from the weld were hot-rolled and swaged to rods of 3 mm diameter and 15 mm length. Some of these cylindrical samples were subsequently drilled along the cylinder axes to give 1.5 mm diameter bores, in order to accelerate the cooling rate that could be achieved during dilatometric experiments. To minimise any effects of chemical segregation, the specimens were then homogenised by annealing at 1200 °C for 3 days while they were protected by sealing in quartz tubes each containing a partial pressure of pure argon. After annealing, the samples were quenched in an ice-water mixture.

The heat treatment studies were mostly carried out in electric resistance heated furnaces (accuracy ± 5 °C). Some of the rapid heat treatments were carried out using high speed dilatometry.

2.3 Dilatometry

The advantage of dilatometry is that it enables transformations to be recorded as they happen. The setup of the sample is explained schematically in Fig. 2.2. The temperatures were measured by a Pt/Pt-Rh thermocouple spot welded to the sample. The volume change associated with a phase transformation can be followed by monitoring the change in length, which over the temperature region of interest can provide information about the transformation temperatures and the reaction kinetics. The length change during transformation was recorded using a *Theta Industries* high-speed dilatometer which is equipped with a water cooled induction furnace which has an essentially zero thermal mass. The intermediate cooling of specimen in dilatometry was carried out using helium gas quench. The dilatometer has been interfaced with a BBC/Acorn computer which is used for programming the thermal cycles and also for automatically collecting and recording length change, time and temperature data. For the dilatometric studies the homogenised specimens were electroplated with 0.08 - 0.1 mm thick layer of nickel to avoid surface degradation and surface nucleation effects (Strangwood and Bhadeshia, 1987c).

The following method is used for calculation of volume fraction of ferrite transformed as a function of time in isothermal transformation studies. The volume fraction of transformation is related to the length change detected by the dilatometer. For bainitic transformation involving no precipitation of carbides, the relation is given by the following equation: (Bhadeshia, 1982b).

$$\frac{\Delta L}{L} \approx \frac{[2V a_\alpha^3 + (1 - V) a_\gamma^3 - \bar{a}_\gamma^3]}{3 \bar{a}_\gamma^3} \quad (2.1)$$

where

$\frac{\Delta L}{L}$ is the relative length change due to transformation, V is the volume fraction of ferrite, a_α is the lattice parameter of ferrite (a function of temperature), which is given by,

$$a_\alpha = \bar{a}_\alpha (1 + e_\alpha(T - 298)) \quad (2.2)$$

where T is the absolute temperature, \bar{a}_α is the lattice parameter of ferrite at ambient temperature (25 °C), e_α is the linear thermal expansion coefficient of ferrite, \bar{a}_γ is the calculated lattice parameter of austenite at the mean alloy composition, i.e., when $V = 0$, it is given by,

$$\bar{a}_\gamma = \left[a_\gamma^\circ + \sum_{i=1}^n C_i x_i \right] [1 + e_\gamma(T - 298)] \quad (2.3)$$

where a_γ° is the lattice parameter of unalloyed austenite, e_γ is the linear thermal expansion coefficient of austenite, C_i are coefficients relating alloying element concentration, x_i , to the lattice parameter, where $i = 1, 2, \dots, n$ denoting various alloying elements ($i = 1$ for carbon). a_γ is the calculated lattice parameter of austenite taking account of the carbon enrichment in austenite when $V \neq 0$ given by,

$$a_\gamma = \left[a_\gamma^\circ + C_1 \frac{(\bar{x} - V x_c^\alpha)}{(1 - V)} + \sum_{i=2}^n C_i x_i \right] [1 + e_\gamma(T - 298)] \quad (2.4)$$

where x_c^α is assumed to be given by the equilibrium concentration of carbon in ferrite in Fe-C alloys, as estimated using an quasichemical thermodynamic model (McLellan and Dunn, 1969, Bhadeshia, 1982c) and \bar{x} is the mean carbon concentration of the alloy in mole fraction. The above method of analysis will be used in the following chapters.

2.4 Lattice Parameters Measurement

The lattice parameter values necessary for the interpretation of dilatometric data were measured for ferrite from samples tempered at 600 °C for one hour, using the Debye-Scherrer X-ray diffraction method with Cu-K α radiation. The accelerating voltage was 45 kV and the tube current being 25 mA. As the Cu-K α_1 and Cu-K α_2 lines could not be resolved, an average wavelength of 1.5424 Å was used for the analysis. A specimen of 0.5 mm diameter was prepared by careful machining from a 3 mm diameter rod, and its surface layer was removed by soaking in a chemical polishing mixture of 5% HF and 50 % H₂O₂ and 45 % H₂O for 10 min; this procedure leads to more accurate parameter measurements since the effects of deformation induced by machining are removed. The Bragg angles were measured from the 011, 002, 112, 022 and 013 reflections and the data plotted against the Nelson-Riley extrapolation function with a least squares linear regression procedure. Since errors decrease with increasing Bragg angle (θ), the data were weighted using a $\frac{1}{\cos^2 \theta}$ function during regression analysis (Cullity, 1978).

2.5 Metallography

2.5.1 Transmission electron microscopy - EDX

The thin foil sample preparation for transmission electron microscope studies was as follows; After slicing 3 mm diameter rods into thin discs of 0.3 mm thickness, the discs were thinned down to 60-80 μm by abrasion using SiC coated grinding paper, and electropolished using an electrolyte consisting of a mixture of 5 % perchloric acid, 25 % glycerol and 70 % ethyl alcohol. The polishing potential was 65 V at a current of 18-25 mA, the electrolyte temperature range being 0-10 °C. The thin foils were examined using a Philips EM-300 or EM-400T transmission electron microscope operated at 100 kV and 120 kV respectively.

Thin film extraction carbon replicas were also prepared for some of the heat treated and weld samples. Replicas were prepared by vapour deposition of carbon on to the sample in a vacuum chamber. The carbon film was stripped off from surface of the sample, by etching away the matrix in 5% chloral (5 % concentrated HCl in ethanol) solution. The replicas were mounted on to copper grids and were observed in TEM.

Thin film foils or replicas were mounted on to a low background specimen holder and tilted to 35° take off angle in the microscope column during energy dispersive X-ray analysis (EDX). The X-ray energy spectra was analysed by LINK - RTS2 analyser program. The program calculates the relative amount of elements present in a test by fitting observed energy spectrum to a standard spectrum. The program is also capable of deconvolving overlapping peaks and giving a thickness correction. The scattering effects in the specimen lead to a beam broadening and was estimated to be around 20 nm with the original spot size being around 2-5 nm.

2.5.2 Scanning Electron Microscopy - EDX

The samples were also imaged in a scanning electron microscope operated at 25 kV and equipped with an energy dispersive X-ray analyser. The specimen was tilted to a take off angle of 45°. The accelerating voltage was reduced to 20 kV for EDX analysis.

2.5.3 Light microscopy and microhardness testing

The sectioned specimens were mechanically polished down to 1 μm finish and etched in 2% nital. Volume fraction measurements were carried out using a Swift point counter at a magnification of 400 \times with 1000 points for each specimen.

The prior austenite grain size for heat treated samples was measured either directly on the metallographic samples when the boundaries were made clearly visible by layers of allotriomorphic ferrite or using a thermal grooving method. In the latter case, metallographically polished specimens were austenitised in a protective helium atmosphere in the dilatometer chamber, and the thermal grooves which develop as the grain boundaries and free surface tension terms

balance, can be used to reveal the positions of the grain boundaries. A micrograph of a thermal grooved specimen is given in Fig. 2.3. The grain sizes were defined using the usual mean linear intercept method. Samples were hardness tested in a Leitz-Vickers microhardness tester with a force of 0.981 N or in macro vickers hardness tester of 50 N load.

2.6 Thermomechanical Simulator

The heat treatment can easily be carried out in the *Formaster* thermomechanical simulator used in the present studies. The machine is equipped to simultaneously monitor and record the diametral and longitudinal strains, in addition to time, temperature and load data. It can be programmed to automatically carry out the specified thermomechanical treatments. The samples were in the form of 8 mm diameter cylinders 12 mm in length, made from the weld metal by rolling, swaging and machining (Fig. 2.4). The specimen was heated using a radio-frequency coil and the temperature was measured with a Pt/Pt-10%Rh thermocouple. The temperature variation along the length of the sample was checked to be within 4-5 °C. The simulator experiments were carried out with the specimen chamber filled with argon.

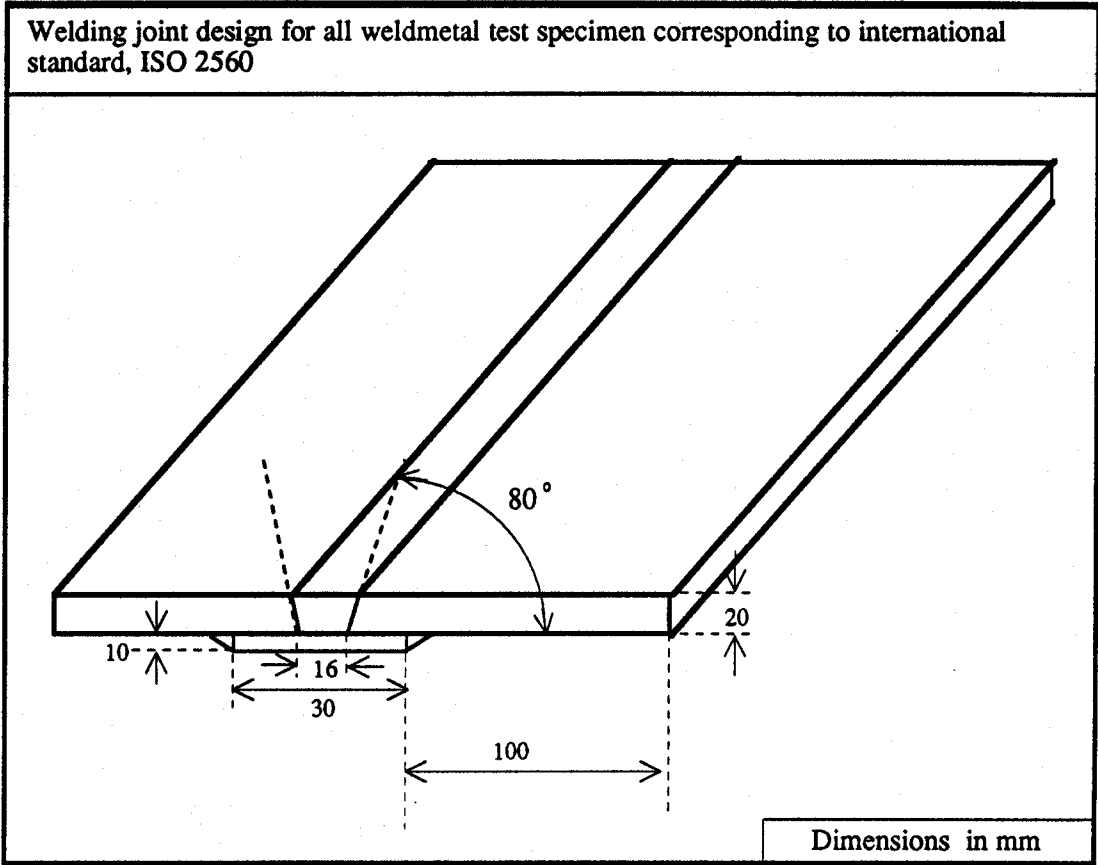


Fig. 2.1 Illustration of all weld metal test specimen, used for preparation of welds, according to ISO 2560.

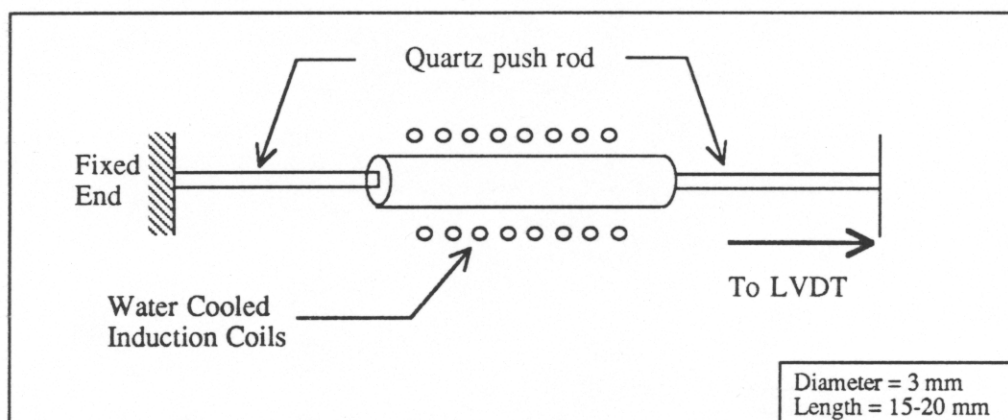


Fig. 2.2 Illustration of specimen set-up in dilatometer. The heating is by RF induction.

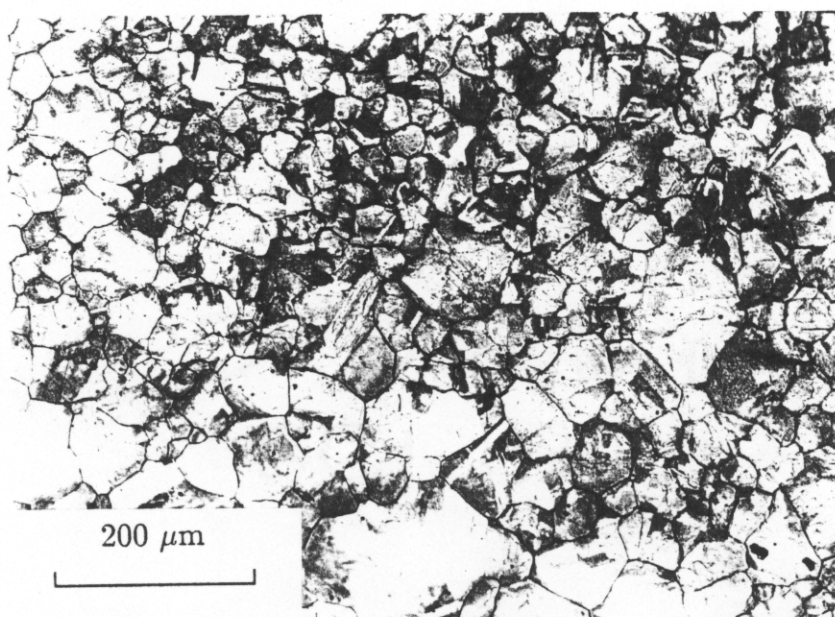


Fig. 2.3 Example micrograph showing the thermal grooving. The polished surface of alloy A78 (see Table 2.2) was austenitised at 1000°C for 10 minutes and cooled rapidly below the bainitic transformation temperature (530°C).

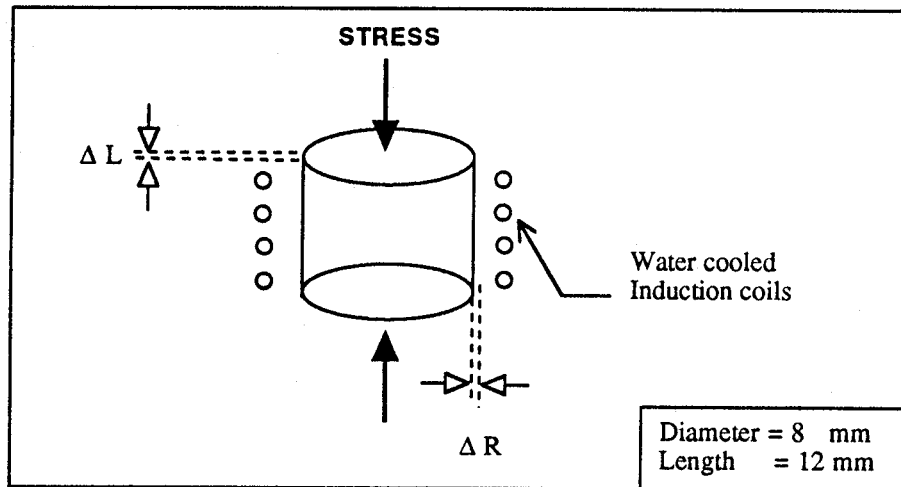


Fig. 2.4 Illustration of specimen set-up in thermo mechanical simulator. The radius change is measured by laser interferometry, the relative length change is measured from the movement of the crosshead.

Chapter 3

The Microstructure of Fe-Cr-C Weld Metals

3.1 Introduction

The effect of systematically increasing only the chromium and molybdenum concentration in the weld metal has been studied quantitatively by Evans (1988, 1986). He found that as the concentration of either of these elements is increased, the amount of allotriomorphic ferrite decreases. The volume fraction of acicular ferrite, however, goes through a maximum. The volume fraction of the remainder of the microstructure, which Evans described as "ferrite with aligned second phase" therefore increases with concentration. This effect is illustrated in Fig. 3.1. The ferrite with aligned second phase actually refers to either or both of bainite and Widmanstätten ferrite. The original diagram by Evans (1988, 1986), has been divided into two regions namely (A) and (B) to illustrate the point that the reduction in α_a may actually arise because acicular ferrite is in increasing quantities replaced by bainite (B). This is supported by the fact that Fe-2.25Cr-1Mo wt.% weld deposits used in the power generation industry exhibit a bainitic structure in the as-deposited condition in spite of the presence of numerous nonmetallic inclusions (Lundin *et al.*, 1986, McGarh *et al.*, 1989 and Josefsson *et al.*, 1987).

This chapter describes an analysis of the published results on Fe-Cr-C welds by Evans (1988) using the weld model developed by Bhadeshia *et al.*, (1985). The second part of the chapter summarises the results of a microstructure study of a series of welds containing chromium. The aim has been to reproduce the behaviour reported by Evans. Observations of the primary weld metal microstructure using transmission electron microscopy are also presented.

3.2 Analysis of Published Data

The welding variables used for microstructural study by Evans (1988) are presented in Table 3.1 & 3.2. The microstructure results were reported for 1.03 wt.% and 1.85 wt.% Mn levels, for a variation of Cr concentration from 0 → 2.3 wt.%. The weld model needs, in addition to the data presented in Table 3.1 and 3.2, the prior austenite grain size (\bar{L}_{tn}) of the welds (see section 1.3.4). The empirical relation developed for the model is only applicable for Fe-Si-Mn-C welds. The results of Evans (1988) did not contain any data on austenite grain size. Hence, the empirical equation (1.15) was applied, by assuming the effect of chromium on the austenite grain size to be minimal.

A comparison of the calculated volume fractions of allotriomorphic ferrite, Widmanstätten ferrite, and acicular ferrite is presented in Fig. 3.2. The figure indicates the poor correlation

Table 3.1 Welding process variables (from Evans ,1988).

Variables	
Welding voltage	21 Volts
Welding current	170 Amps
Welding speed	0.0027 m s ⁻¹
Interpass temperature	250 °C
Welding process	MMA

Table 3.2 Weld metal composition (in wt.%).

ALLOY	C	Si	Mn	Ni	Mo	Cr	O _(ppm)	N _(ppm)
E1	0.037	0.31	1.03	0.0	0.0	0.0	-†	-†
E2	0.041	0.32	1.01	0.0	0.0	0.24	-	-
E3	0.043	0.31	0.95	0.0	0.0	0.53	-	-
E4	0.045	0.32	0.97	0.0	0.0	1.04	-	-
E5	0.046	0.30	0.93	0.0	0.0	2.38	-	-
E6	0.045	0.33	1.85	0.0	0.0	0.0	-	-
E7	0.048	0.33	1.85	0.0	0.0	0.24	-	-
E8	0.051	0.33	1.83	0.0	0.0	0.53	-	-
E9	0.052	0.33	1.81	0.0	0.0	1.08	-	-
E10	0.054	0.33	1.72	0.0	0.0	2.32	-	-

†Oxygen concentration and nitrogen concentration were taken as 300 ppm and 100 ppm respectively for the calculations. The estimated prior austenite grain size for welds E1-10 was in the range of 140-150 μm using the equation 1.15.

obtained in prediction of the allotriomorphic ferrite and acicular ferrite. The deviation is evident in high Cr welds, where the transition from acicular ferrite to bainite was observed.

3.3 Experimentation

The transition from acicular ferrite to bainite can be attributed to either a reduction

in austenite grain size (Yang and Bhadeshia, 1987a) or a change in inclusion characteristics (Harrison and Farrar, 1981). The analysis of the above parameters were not reported by Evans (1988). Thus, the present work concentrated on study of austenite grain size and inclusion characteristics in a series of Cr welds. All weld metal test pieces were fabricated (Table 2.1) with different chromium levels using the procedure described in chapter 2. The Cr content in weld was varied from 0.48 wt.% (Table 2.2). Optical microscopy and scanning electron microscopy were used to characterise the microstructure, in transverse sections of the welds. Measurements of the prior austenite grain size were carried out by drawing test lines perpendicular to the major axes of the columnar grains, consistent with the approach of Svensson *et al.*, (1986). The delineation of prior austenite grain boundaries by allotriomorphic ferrite made their identification relatively easy. In alloy 77, the austenite grain boundaries were very faint in the absence of allotriomorphic ferrite.

Specimens of the primary microstructure, were prepared as thin foils for transmission electron microscopy. Around 20 inclusions were microanalysed from each weld. Carbon film extraction replicas were used to measure the inclusion size distributions (100 inclusions per each weld).

3.4 Results and Discussion

3.4.1 Austenite grain size variation with chromium content in weld

The columnar austenite grain structures of the welds are shown in Fig. 3.3 and quantitative data in Fig. 3.4. The austenite grain size appears to increase with the chromium concentration, although the variations are in fact within the standard deviation given in Table 3.3. The small grain size of alloy 77 can in fact be attributed to its larger carbon concentration (equation 1.15) rather than to its chromium concentration. Thus, it has to be concluded that the changes in austenite grain sizes cannot explain the peak in α_a content as the chromium concentration is increased.

3.4.2 Weld Metal Microstructure

It is evident from Fig. 3.5 that as the chromium content increases, the amount of acicular ferrite increases at the expense of allotriomorphic ferrite. However, after 1 wt.% Cr level the microstructure became very fine. The optical microstructure in alloy 77 indicated the presence of parallel sheaves of fine plates in most of the regions, consistent with Evans' (1988) results. It was found that the calculated volume fraction of allotriomorphic ferrite (Bhadeshia *et al.*, 1985) was always greater than that measured (Table 3.4). The weld model predicted correctly the absence of allotriomorphic ferrite in alloy 77. In alloy 78, allotriomorphic ferrite was found to be discontinuous whereas the calculations are based on the assumption of uniformly covered

Table 3.3 Comparison of austenite grain sizes.

ALLOY	Mean Linear Intercept \bar{L}_{tn} in μm		
	Measured	Standard Deviation	Calculated
80	91	21	111
79	97	22	114
78	110	28	114
77	85	17	77

austenite grain boundaries.

Continuous Cooling Transformation (CCT) diagrams are useful in understanding the development of microstructure. Using the calculated TTT diagrams (Bhadeshia, 1982a), the CCT diagrams were estimated using the additive reaction rule for all the Cr welds (Fig. 3.6). The calculations represent the transformation start temperatures for different cooling rates. They indicate the inability of alloy 77 to form allotriomorphic ferrite for a typical cooling rate of 50°Cs^{-1} . The sensitivity of allotriomorphic ferrite formation to the cooling rate can be seen from the CCT diagrams. Thus, the incomplete coverage of γ boundaries by allotriomorphic ferrite observed in alloy 78 can be attributed to its higher hardenability. The weld model correctly predicts the observed trend in allotriomorphic ferrite fraction, although the accuracy could be improved. The amount of Widmanstätten ferrite decreased with increasing chromium concentration in a way consistent with the results of Bhadeshia *et al.*, (1986c). Similar to Evans' (1988) results at high Cr concentration, the weld metal microstructure became finer. Transmission electron microscopy confirmed that alloys 80 and 79 contain acicular ferrite (Fig. 3.7). The plates nucleate from inclusions and probably also sympathetically from previously formed ferrite plates. Alloy 78 exhibited a mixed acicular ferrite and bainitic microstructure. Fig. 3.8a shows an acicular ferrite colony. Fig. 3.8b shows a dark field image of an acicular ferrite illustrating extensive dislocation networks. Figure 3.8c illustrates bainitic ferrite sheaves emanating from a prior austenite grain boundary. Alloy 77 showed a lesser tendency for acicular ferrite development, with considerable grain boundary nucleated bainitic ferrite (Fig. 3.8d). Figure 3.8e shows the sheaf structure of bainite comprising of many sub-units, a typical bainitic structure. Occasionally ferrite plates developing from inclusions were also observed (Fig. 3.8f), even in alloy 77.

Table 3.4 Microstructural constituents in the welds containing chromium.

ALLOY	Microstructural component in %							
	α		α_W		α_a		α_b	
	exp.	calc.	exp.	calc.	exp.	calc.	exp.	calc.
80	25	28	26	20	49	52	NO	NC
79	21	24	12	19	64	57	3	NC
78†	5	20	NO	15	$\simeq 60$	65	$\simeq 35$	NC
77†	NO	0	NO	0	NO	100	$\simeq 100$	NC

exp. → experimental determination (point count analysis),

calc. → calculated using Bhadeshia *et al.*, (1985) model,

α → allotriomorphic ferrite,

α_W → Widmanstätten ferrite,

α_a → acicular ferrite,

α_b → bainitic ferrite,

NC → not calculated.

NO → not observed

† difficulties in resolving the microstructure using optical microscopy.

The microstructural observations suggest a competition between grain boundary nucleated bainite and acicular ferrite (intragranularly nucleated bainite) as a function of Cr. At high concentrations, the bainite reaction dominates. In other words, the formation of acicular ferrite is stifled by that of bainite as the Cr concentration increases.

The possible reasons for the above transition have to be explored, to design welding variables such that acicular ferrite can be introduced in high Cr welds. Bainitic ferrite is encouraged if the number density of grain boundary nucleation sites increases; acicular ferrite on the other hand is stimulated by an increase in the number density of intragranular nucleation sites (inclusions). Thus, the transition may be related to a change in the relative number densities of inclusion and γ grain boundary nucleation sites, or by some change in inclusions characteristics as the Cr concentration changes.

The measured inclusion compositions (Table 3.5) indicate no systematic or significant

Table 3.5 Comparison of mean inclusion composition determined by TEM-EDX on thin foils of the primary weld metal deposits in wt.%.

Alloy	Cr	Si	Mn	Ti †	Al	Fe	S
80	0.4	20.5	41.5	6.3	1.1	30.1	2.0
79	1.1	20.5	36.5	5.7	1.2	32.8	1.6
78	0.9	21.7	40.5	5.4	1.7	28.3	1.7
77	1.5	14.6	36.1	8.7	1.8	36.7	0.9

†maximum amount of titanium present in the inclusions were 15, 13, 16 and 25 wt.% in alloy 80, 79, 78 and 77 respectively.

change within the alloys studied. It can be deduced that the inclusions are complex silico-manganese oxides (the high concentration of iron may be an effect due to interference from the matrix during microanalysis). Relatively few inclusions were found to be rich in titanium. The inclusion number density is usually related to the oxygen present in the welds (Harrison and Farrar, 1981), which does not vary much (Table 2.2). Hence, a change in number density or size distribution is not expected. A detailed analysis of inclusions is summarised in Fig. 3.9 and Fig. 3.10. This reveals no change in the inclusion characteristics.

3.5 Summary

Published data on the effect of Cr and Mo on the primary weld microstructure have been analysed and it has been suggested that the reported "ferrite with second phase" at higher Cr levels is mainly bainitic ferrite. The weld model correctly predicts the experimental trend. Deviation from the microstructure model is found to be most marked at higher Cr concentration levels.

It has been demonstrated that the microstructure at higher Cr levels is bainitic in nature. There is a competition between intragranular nucleation and grain boundary nucleation; the latter dominates at higher Cr levels. No significant changes in austenite grain size and the inclusion characteristics were observed. In summary, the transition from acicular ferrite to bainite, observed as a function of Cr in welds, can neither be related solely to the austenite grain size, nor to any change in the inclusion characteristics. The indications are therefore that there must be an increase in the grain boundary nucleation of bainite, as the Cr concentration is increased. This hypothesis is investigated in detail in chapter 4.

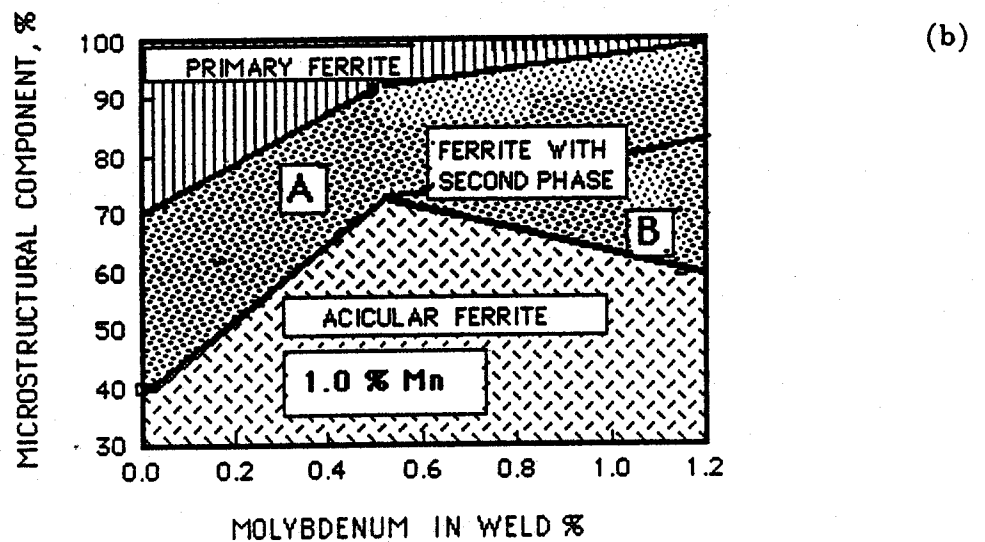
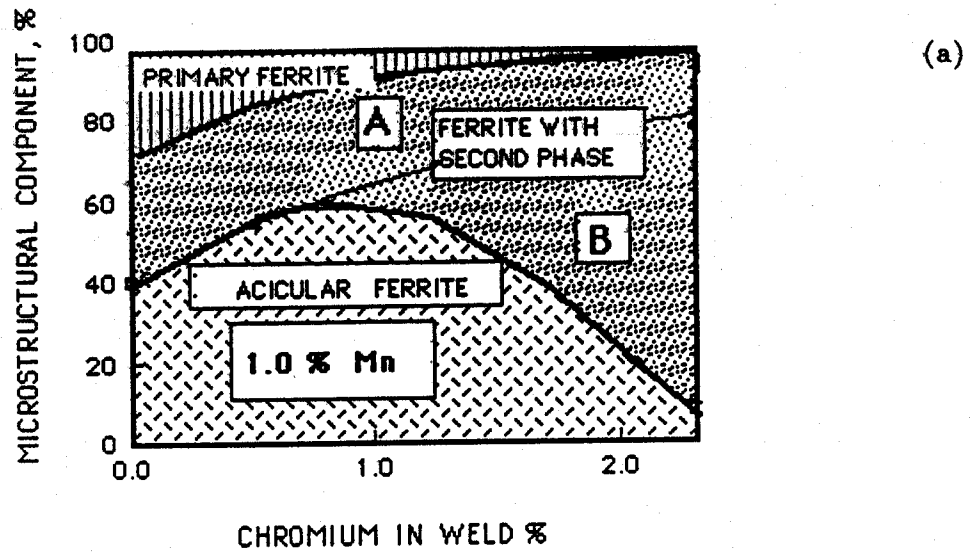


Fig. 3.1 Illustration of the effect of chromium and molybdenum on C - Mn primary weld metal microstructure (Evans, 1988, 1986). The region "ferrite with second phase", is divided into two regions to indicate the expected behaviour. The region "B" represents bainite. (a) effect of Cr, (b) effect of Mo.

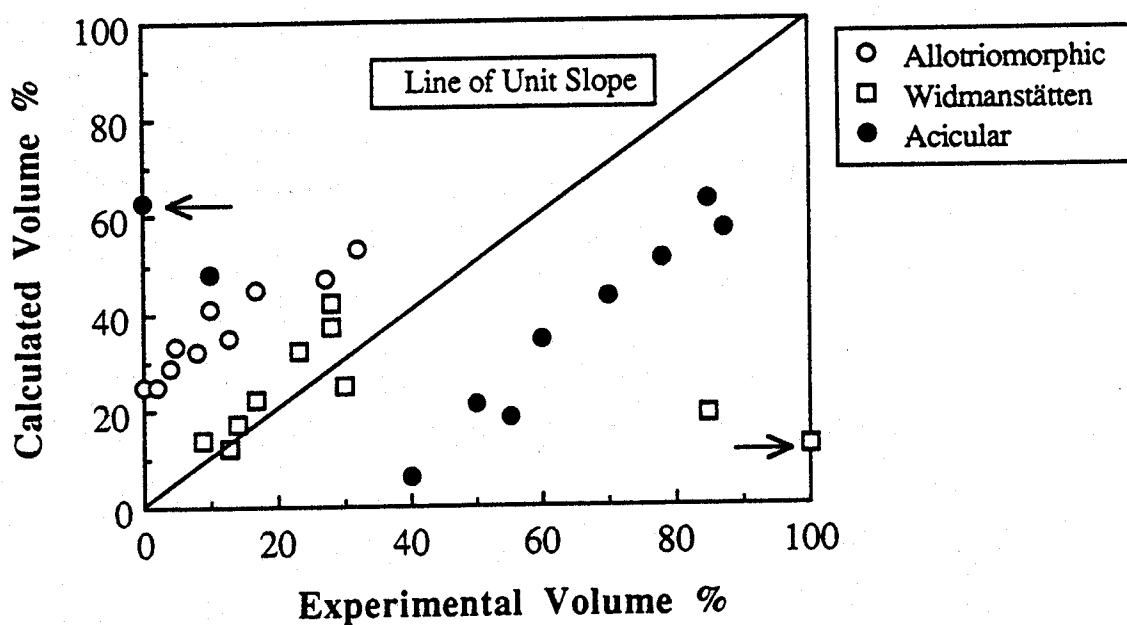
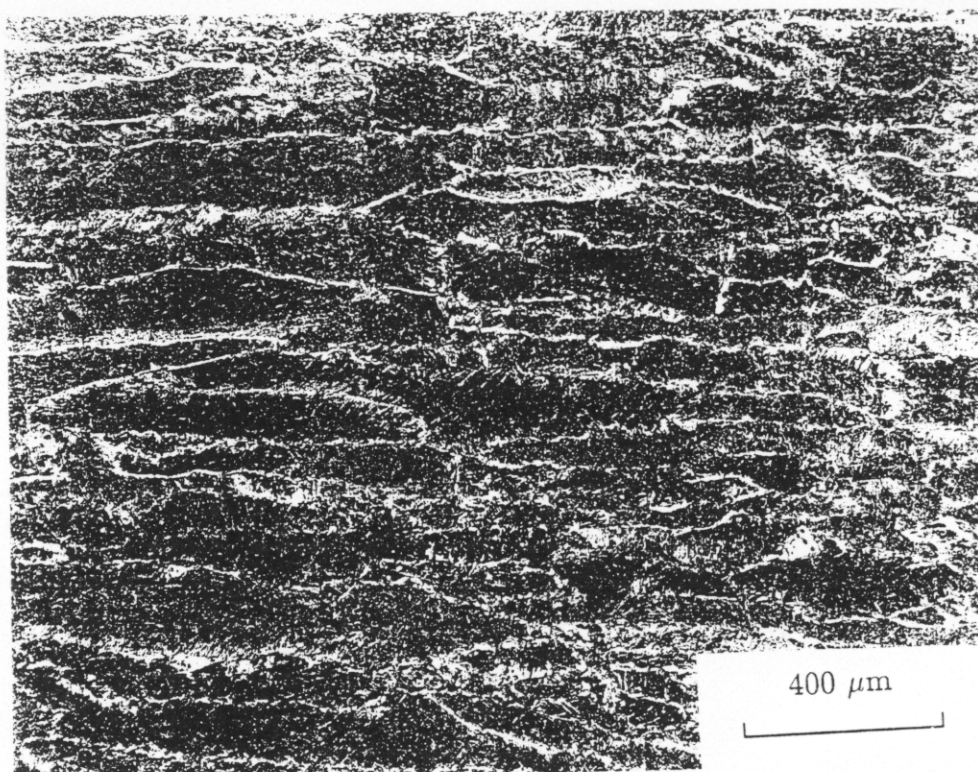
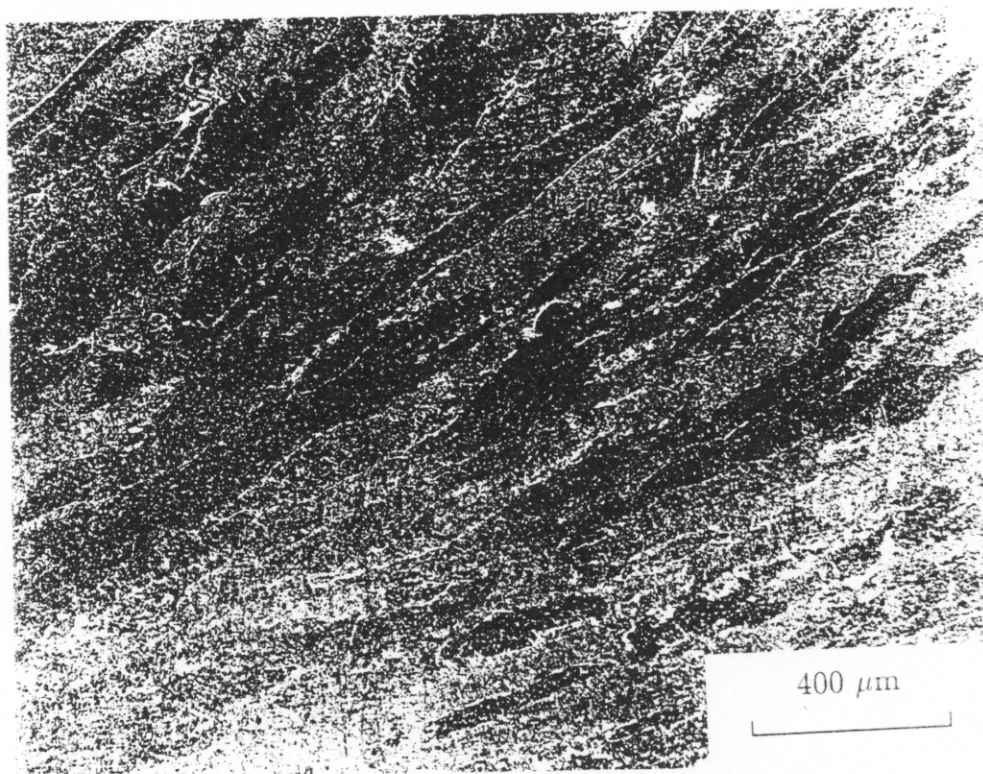


Fig. 3.2 Comparison of published data (Evans, 1988) with calculated microstructures. "Ferrite with second phase" (terminology of Evans) is represented as Widmanstätten ferrite, for comparison only. The classification of microstructure as ferrite with second phase at high Cr levels is not correct, as the microstructure becomes bainitic. The arrows in the case of acicular ferrite and Widmanstätten ferrite comparison correspond to the state of high Cr, where the microstructure is essentially bainitic.



(a)



(b)

Fig. 3.3 Comparison of the austenite grain structure development in the primary weld metal region as chromium content increases. Note the fine microstructure development in the case of alloy 77 and reduced grain boundary allotriomorphic ferrite delineation for alloy 78. (a) Alloy 80, (b) Alloy 79, (c) Alloy 78, (d) Alloy 77.

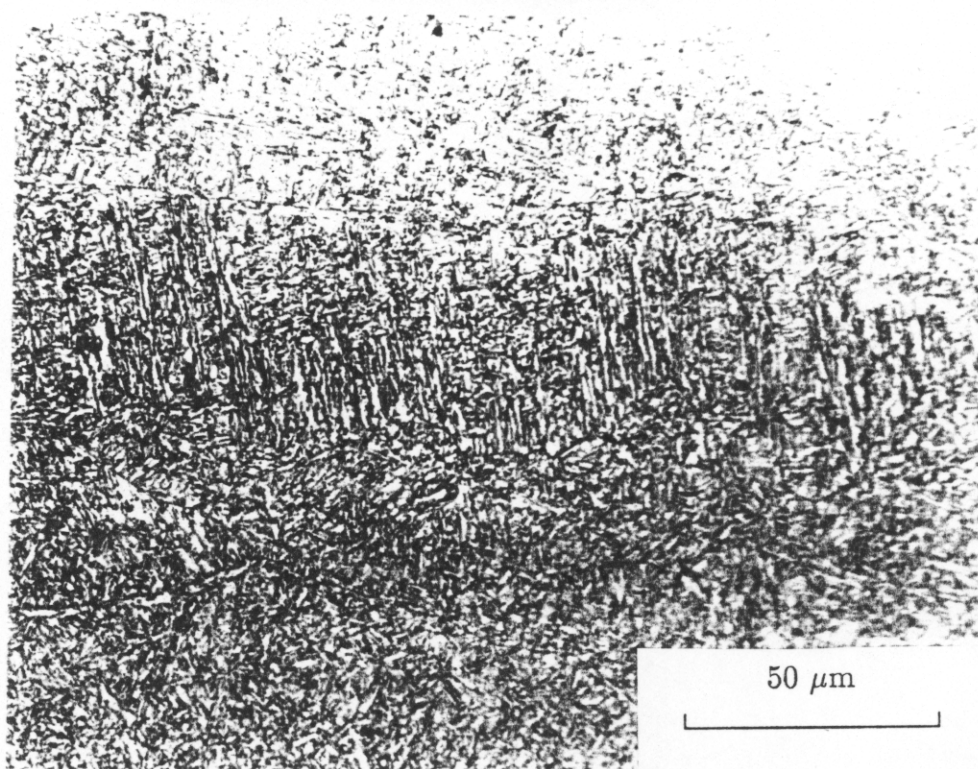
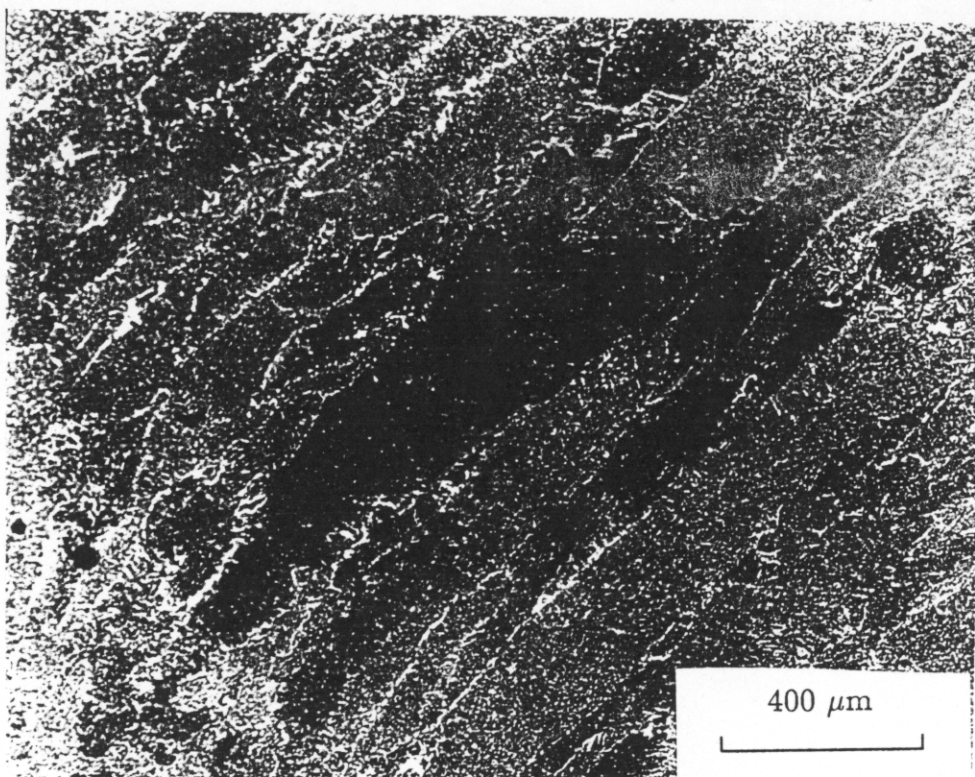


Fig. 3.3 continued....

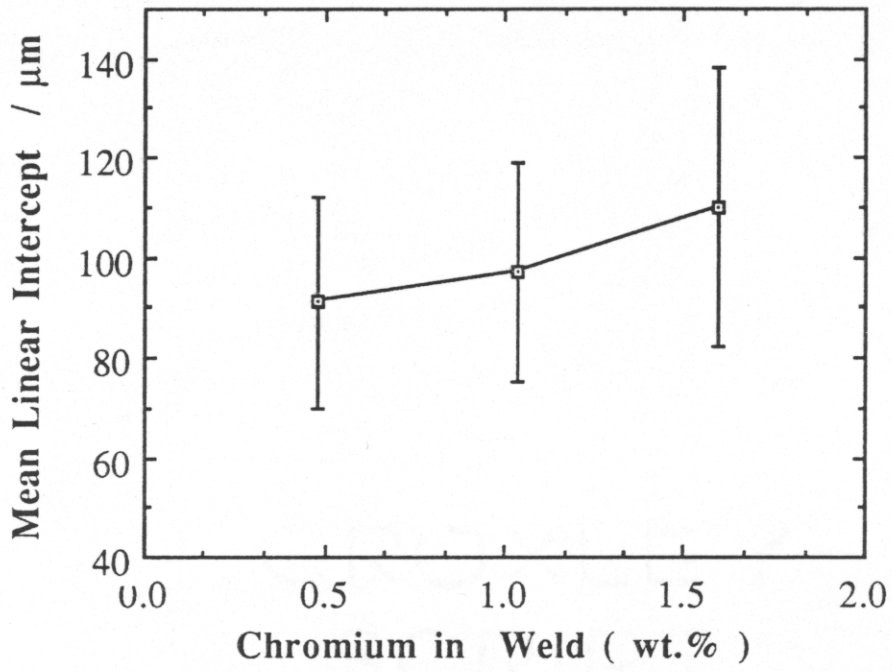


Fig. 3.4 Prior austenite grain size (\bar{L}_{tn}) for different weld Cr concentrations.

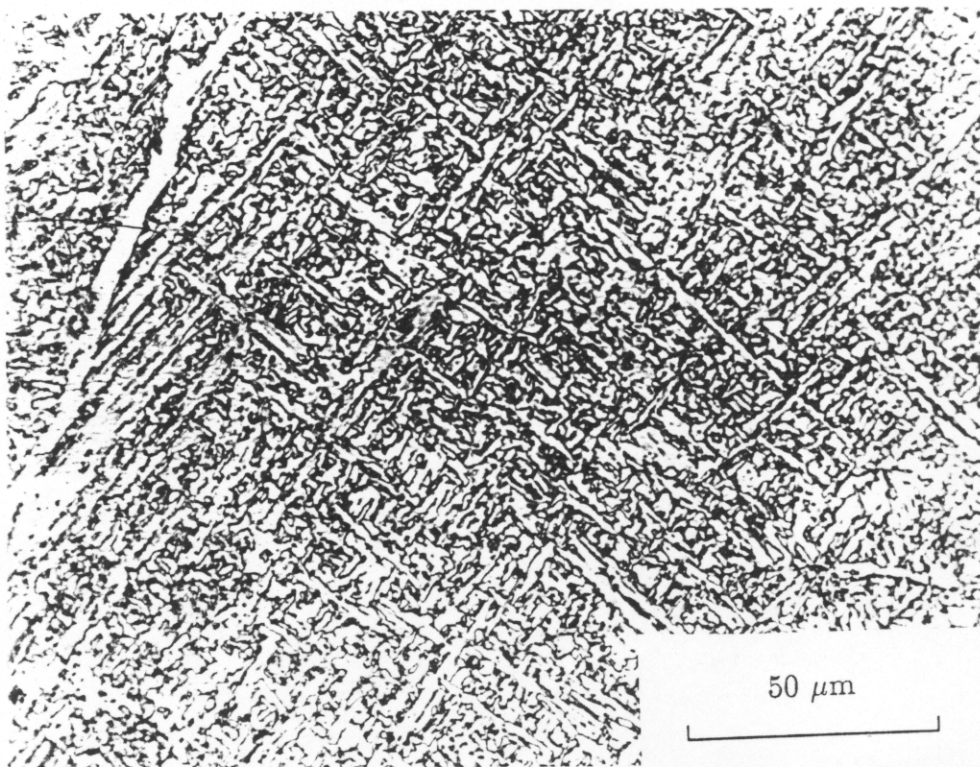
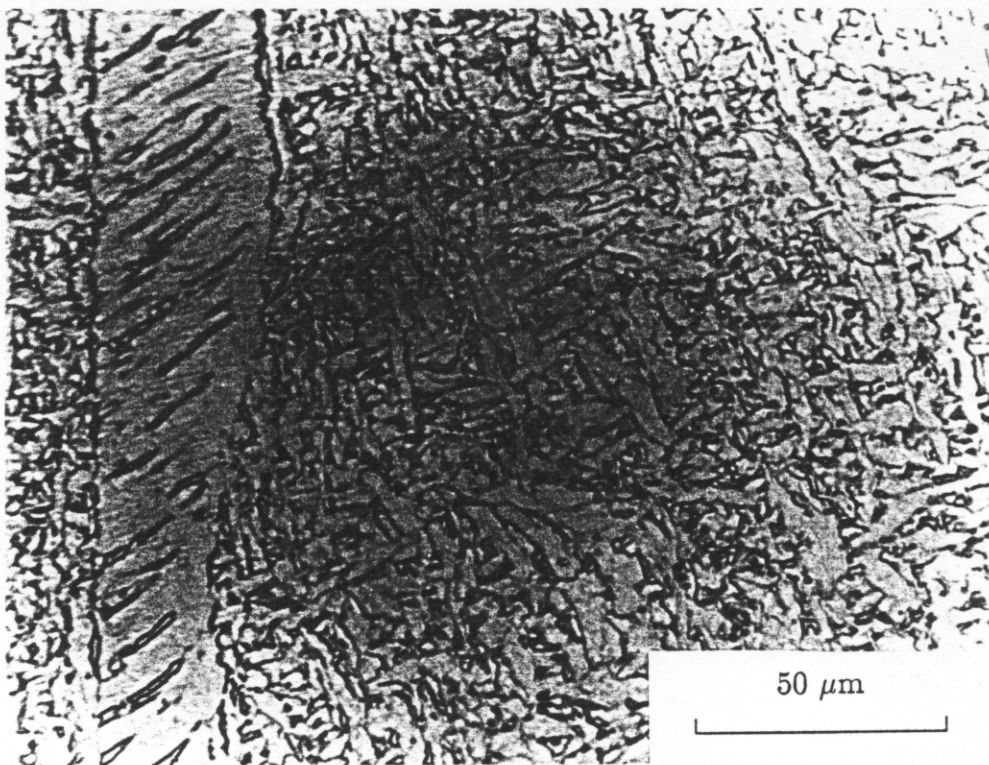


Fig. 3.5 Comparison of the primary weld metal microstructure as the chromium content increases; (a) Alloy 80, (b) Alloy 79, (c) Alloy 78, (d) Alloy 77.

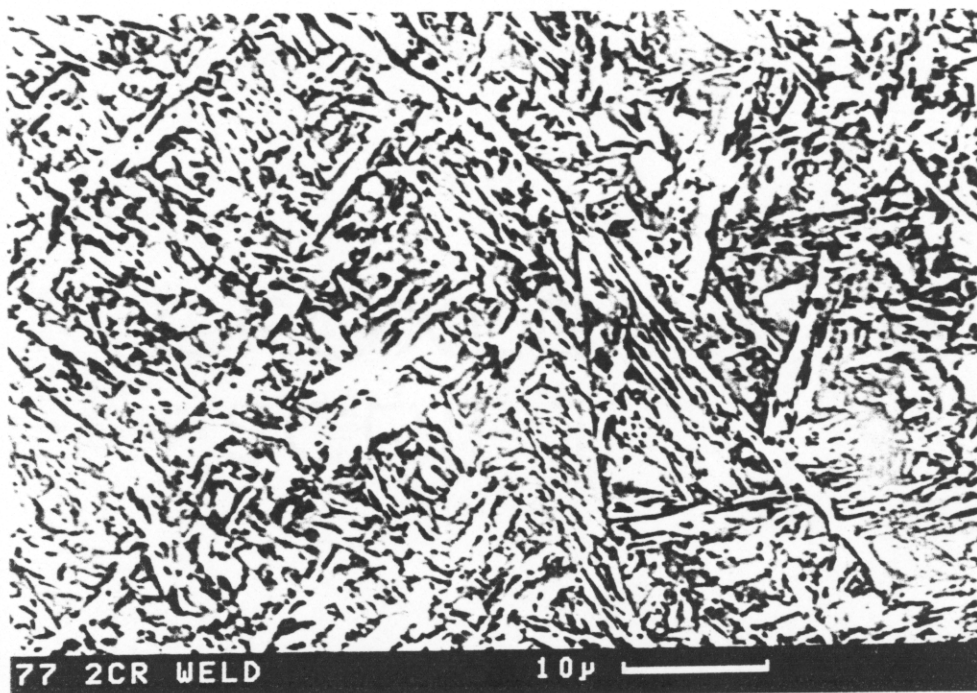
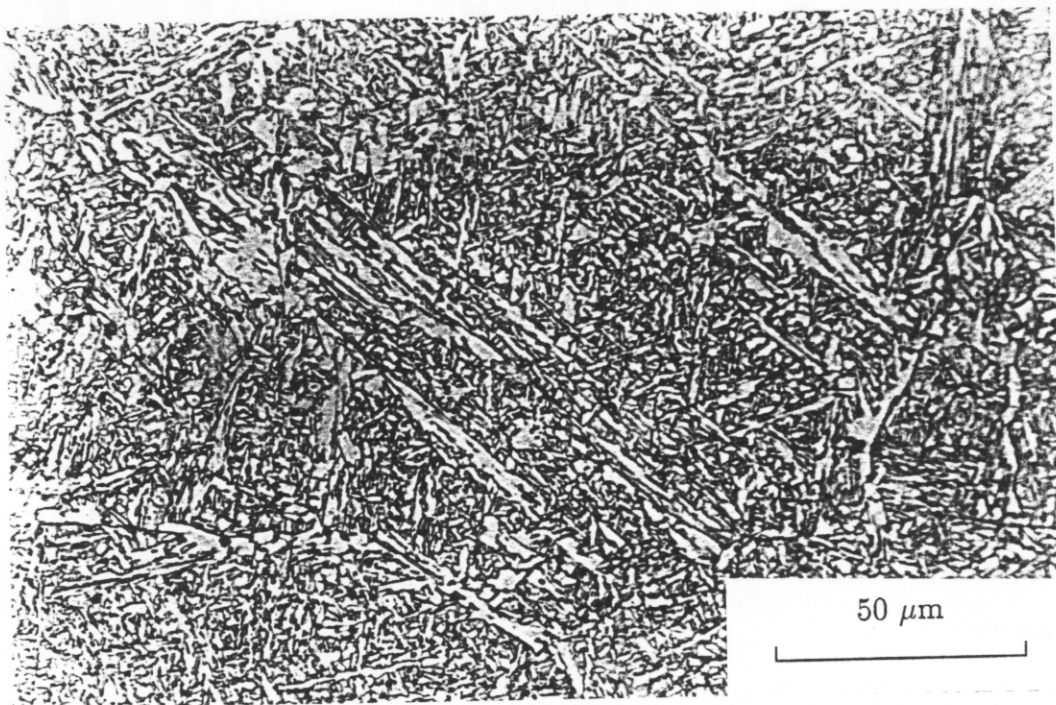


Fig. 3.5 continued...

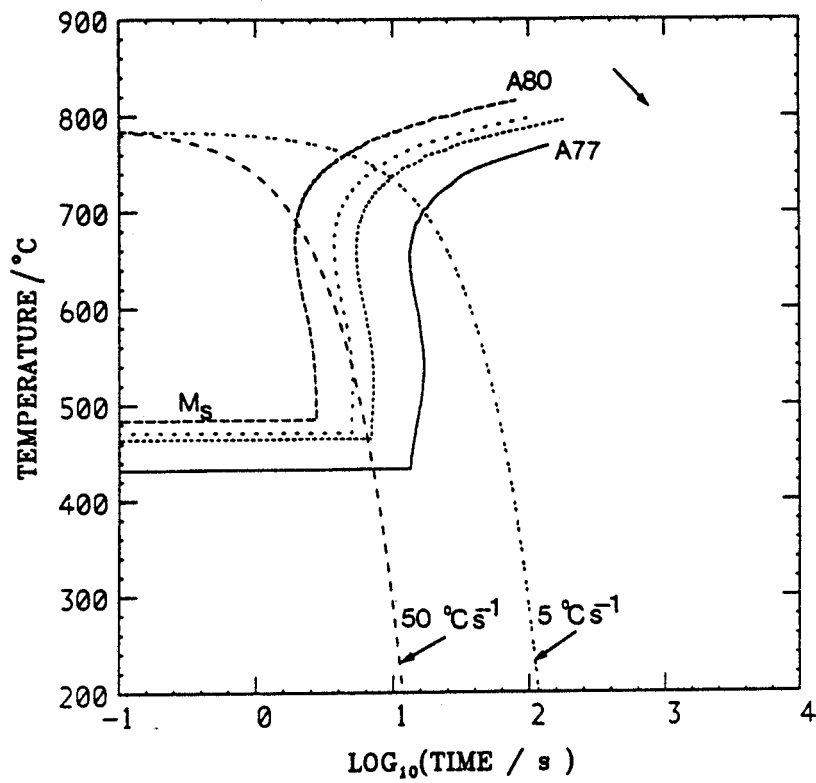
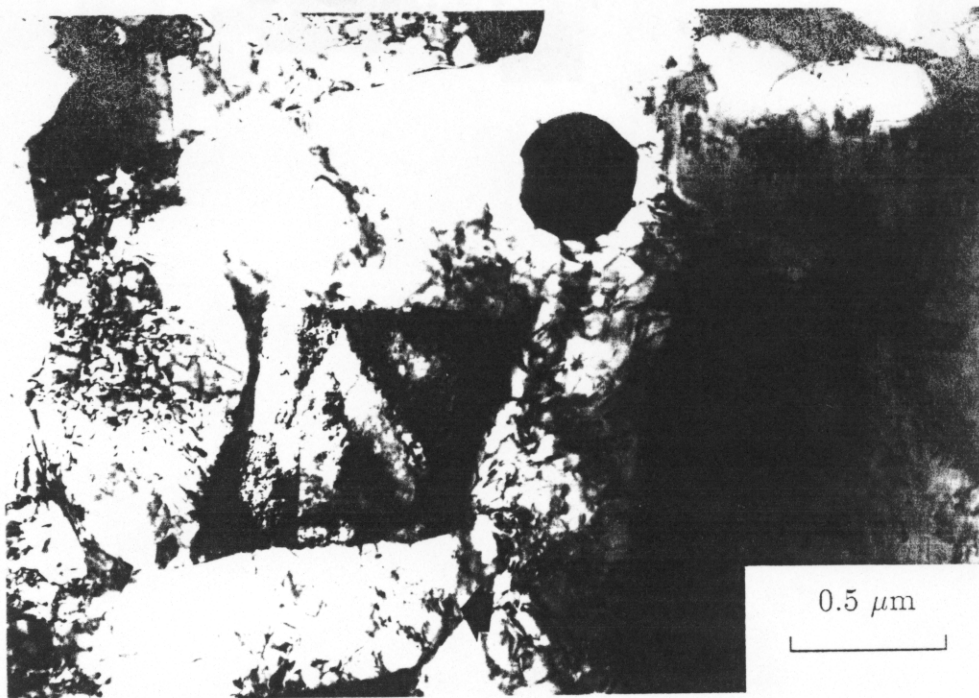
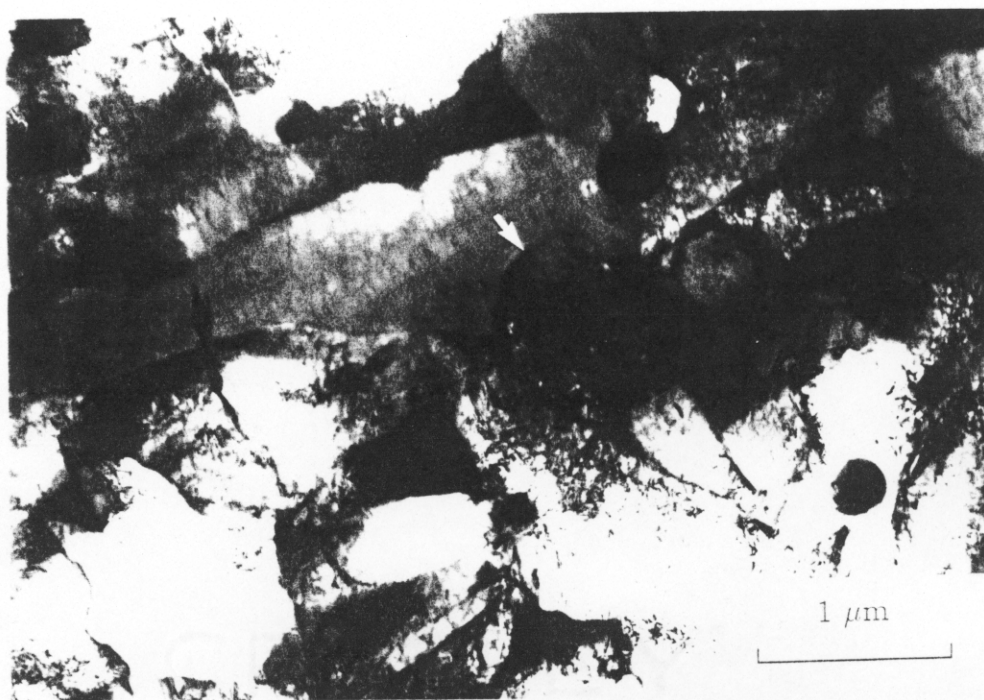


Fig. 3.6 Comparison of CCT diagrams from TTT data calculated using the method developed by Bhadeshia (1982a). The two cooling curves shown are for $5\text{ }^{\circ}\text{C s}^{-1}$ and $50\text{ }^{\circ}\text{C s}^{-1}$. The CCT diagrams were calculated using the additivity reaction rule (Christian, 1975)



(a)



(b)

Fig. 3.7 Comparison of the primary weld metal microstructures of alloy 80 and alloy 79.

- (a) Acicular ferrite microstructure (arrow marks the region of possible sympathetic nucleation).
- (b) Acicular ferrite colony in alloy 79. Sympathetic nucleation is again evident.

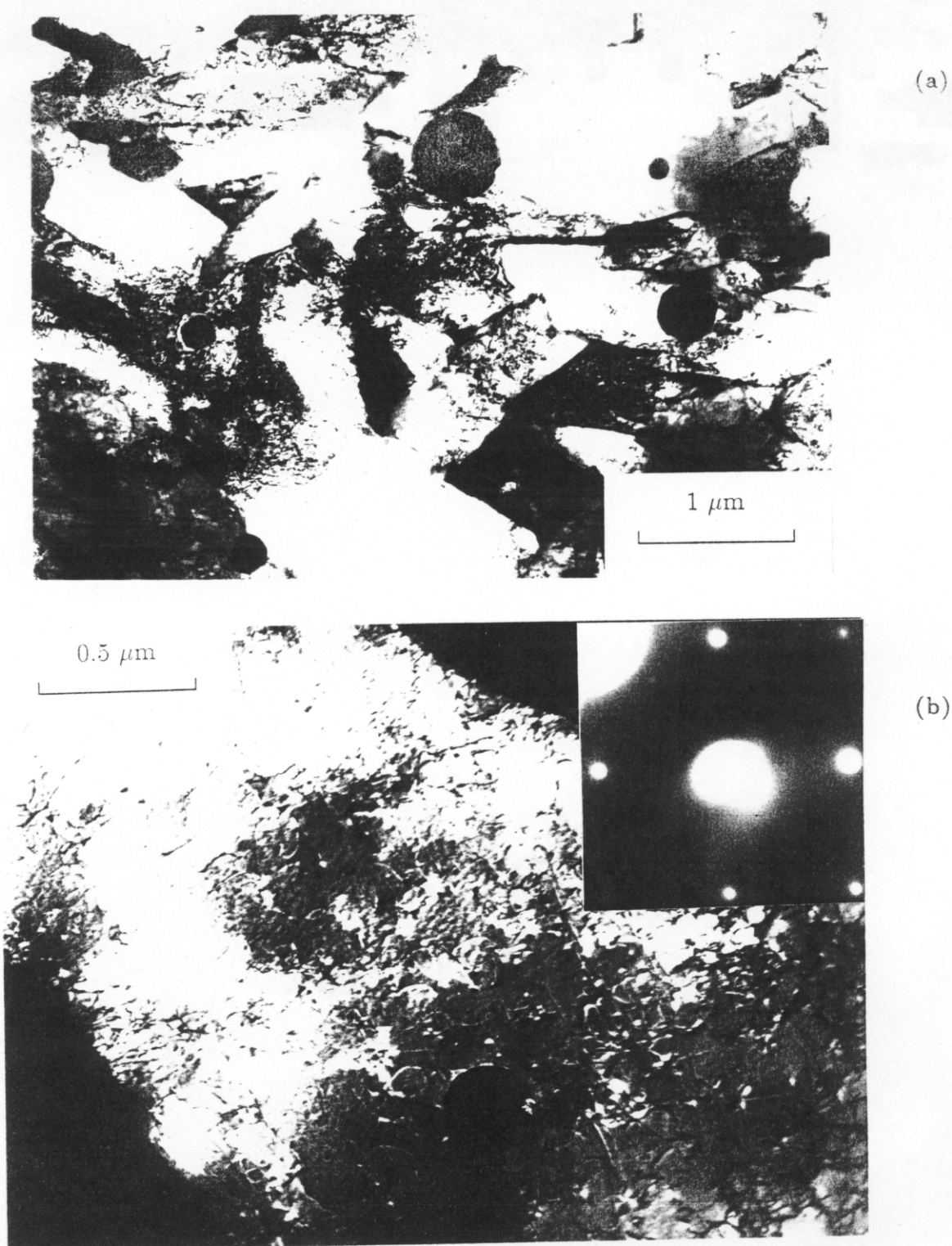
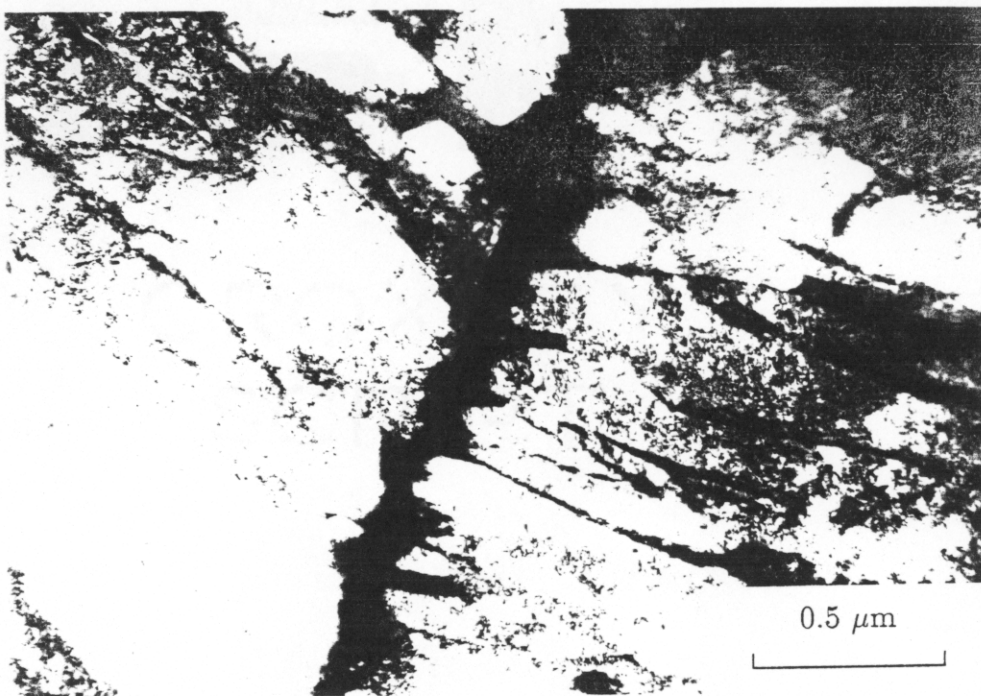
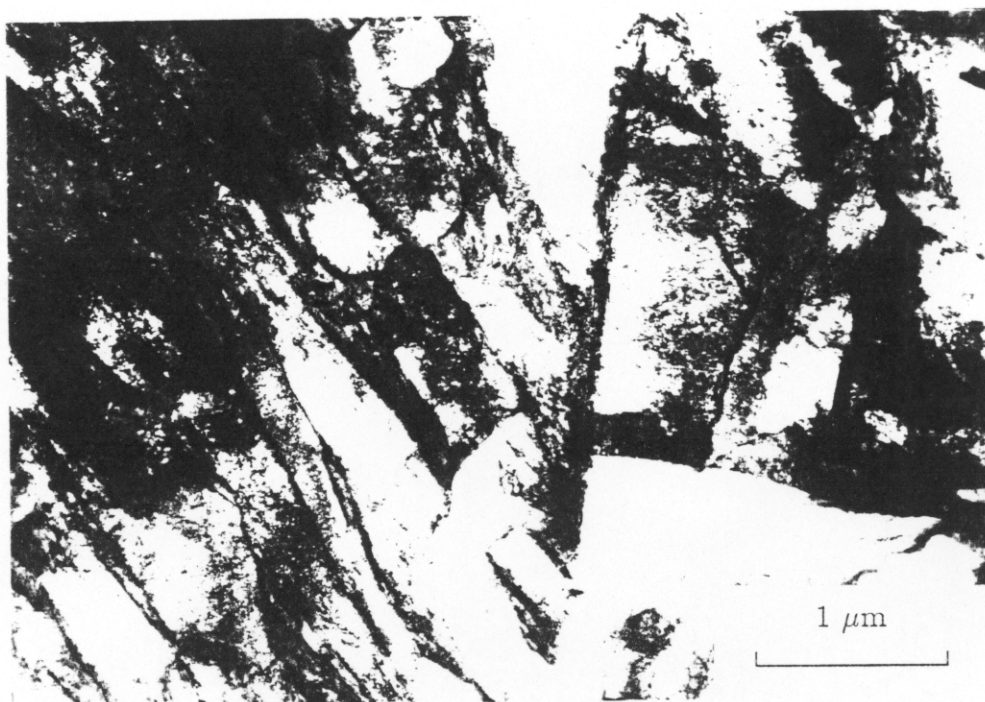


Fig. 3.8 Comparison of the primary weld metal microstructures of alloy 78 and alloy 77.

- (a) Acicular ferrite colony in the weld metal region of alloy 78.
- (b) Centered dark field image, using a (110) reflection of an acicular ferrite plate with a high dislocation density (alloy 78).



(c)



(d)

Fig. 3.8 continued...

- (c) Bainitic ferrite sheaf emanating from a prior austenite grain boundary (alloy 78).
- (d) Bainitic ferrite sheaf emanating from a prior austenite grain boundary (alloy 77).

(e)

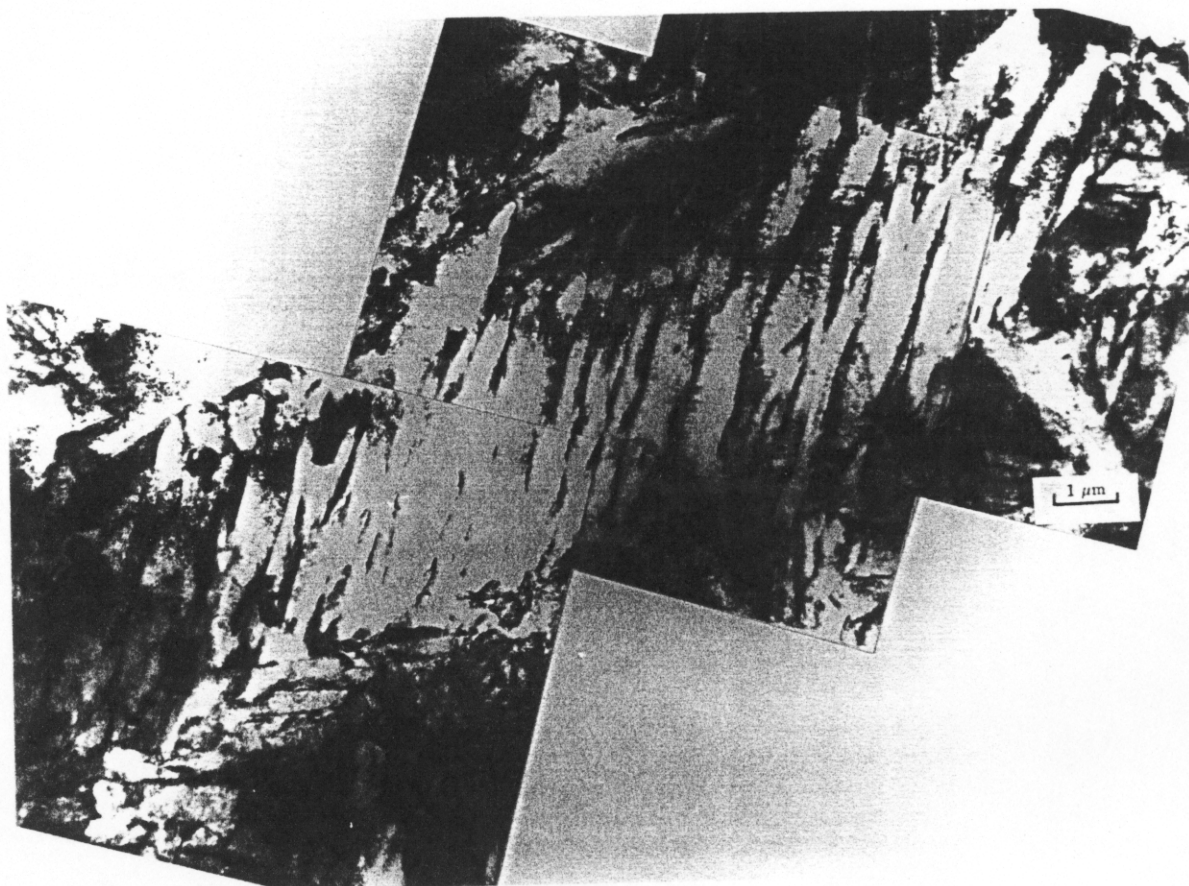
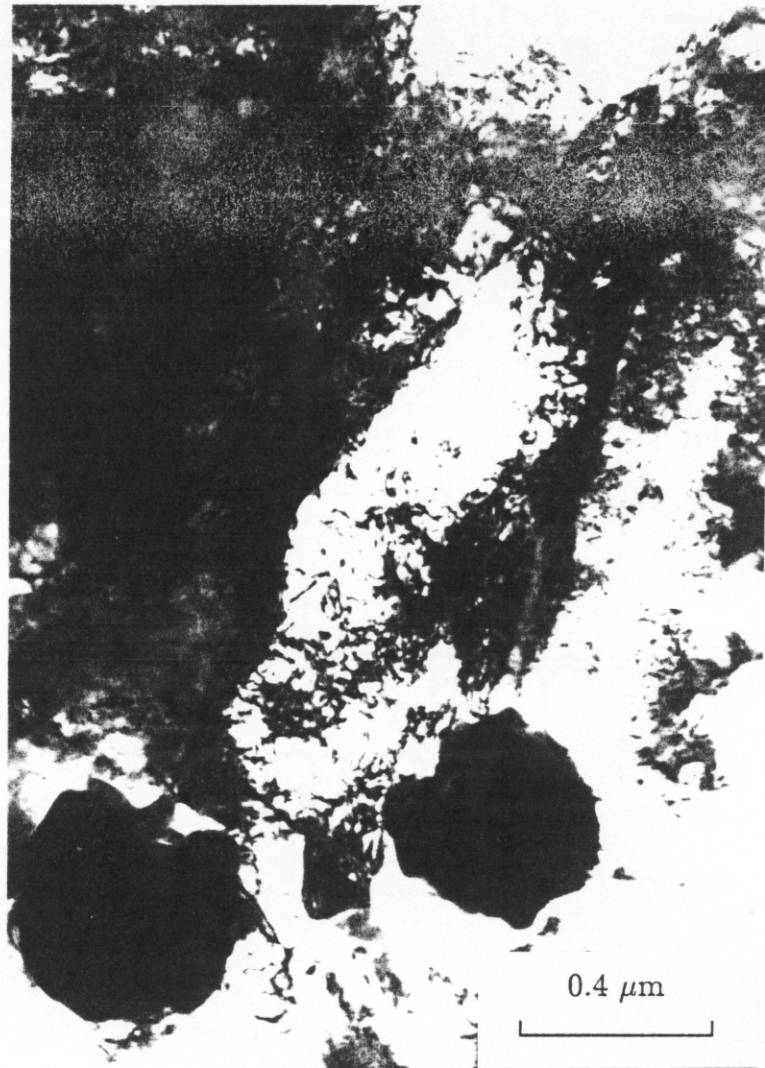


Fig. 3.8 continued...

(e) Another example of a bainitic sheaf structure in alloy 77.



(f)

(f) Bright field transmission electron micrograph of acicular ferrite plate in alloy 77. Direct nucleation on an inclusion can be observed.

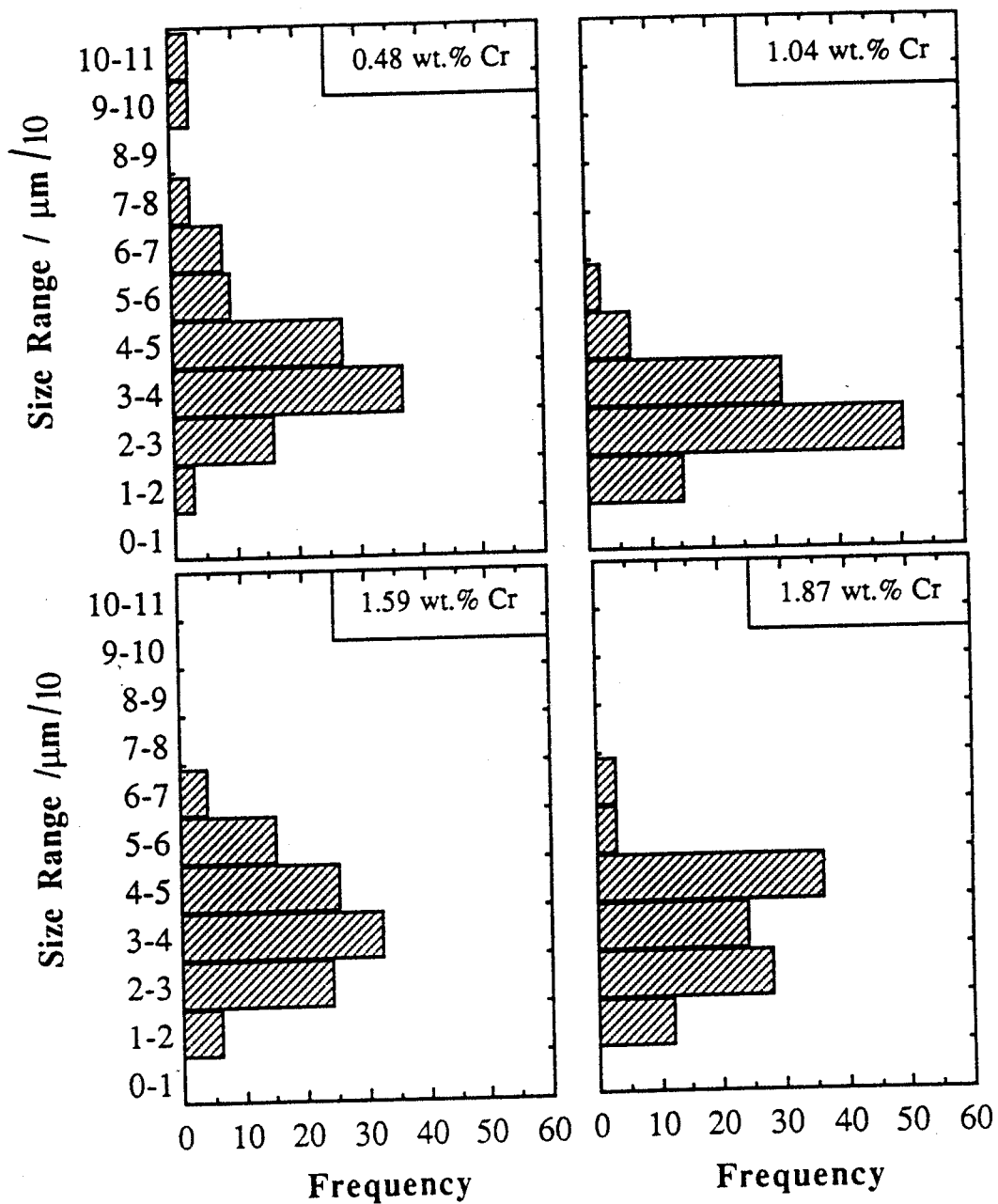


Fig. 3.9 Comparison of the size distributions of inclusions in the weld, illustrating no apparent change with the Cr concentration.

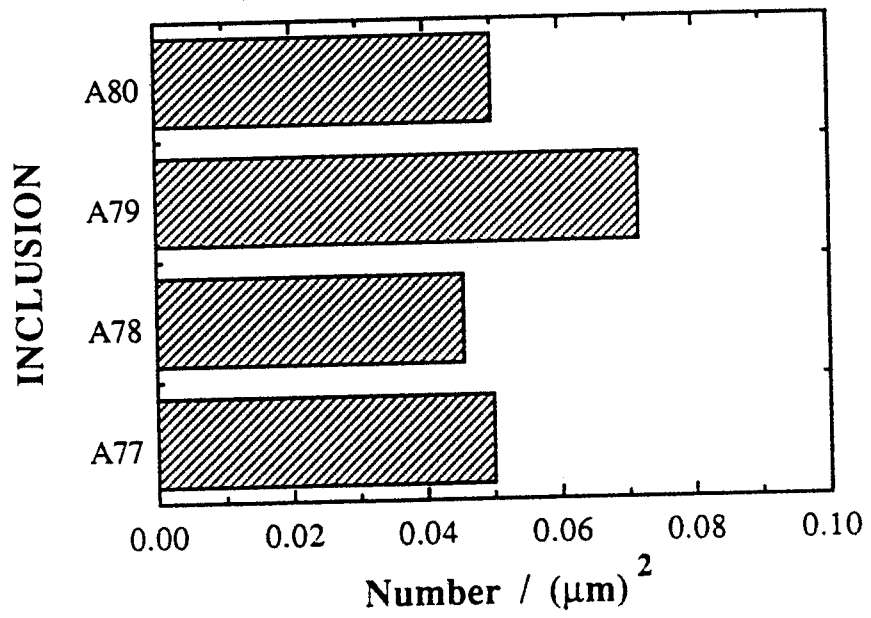


Fig. 3.10 Comparison of the number density of inclusions in the weld, illustrating no apparent change with the Cr concentration. The units on the 'X' axis correspond to the number of inclusions per unit area measured in extraction replicas.

Chapter 4

The Transition from Bainite to Acicular Ferrite in Reheated Fe - Cr - C Weld Deposits

4.1 Introduction

In many steel weld deposits, a reduction of allotriomorphic ferrite and Widmanstätten ferrite leads to a corresponding increase in the amount of acicular ferrite. This behaviour has been demonstrated to be consistent with phase transformation theory. It has been suggested however, that there is a peculiarity in the development of microstructure in Fe-Cr-Mo-C weld deposits (Bhadeshia, 1989, Evans, 1988 & chapter 3). The bainitic microstructure was observed at high alloy contents (see Fig. 3.1). In the previous chapter on the microstructure development in Fe-Cr-C welds the transition from acicular ferrite to bainite was observed. †

Recent work on acicular ferrite (Yang and Bhadeshia, 1987a & Strangwood and Bhadeshia, 1987a) indicates that acicular ferrite appears to be *intragranularly nucleated bainite*, in which the development of aggregates of parallel plates (the classical sheaves of bainite) is suppressed by the hard impingement of acicular ferrite plates nucleating from adjacent sites. Thus, bainite sheaves develop when they can nucleate at the austenite grain surfaces, whereas the intragranularly nucleated bainite is, in effect, acicular ferrite. Thus, a reduction in inclusion density leads to a transition from acicular ferrite to bainite as demonstrated by Harrison and Farrar (1981). Alternatively, an increase in the density of austenite grain boundary nucleation sites leads to the same transition (Yang and Bhadeshia, 1987a). These studies emphasise the dependence of the transition on the relative amounts of austenite grain boundary and intragranular nucleation sites available when the weld metal reaches a transformation temperature below the bainite-start temperature B_s .

Based on this current knowledge on the factors favouring bainite versus acicular ferrite, it was considered that bainitic microstructure begins to dominate at high solute concentration, perhaps because the usual allotriomorphic ferrite layers then begin to diminish, leaving the austenite grain surfaces exposed for the nucleation of bainite. Therefore, the work reported here had the intention of identifying any role of allotriomorphic ferrite in the transition from a predominantly bainitic microstructure to one containing a large amount of acicular ferrite. Allotriomorphic ferrite grows as layers on the prior austenite grain boundaries and, since it is the first phase to grow on cooling from the austenite phase field, it should cause a reduction in the number density of austenite grain boundary nucleation sites and, hence, promote the

† Here the word transition means, the austenite instead of transforming to acicular ferrite transforms to bainitic ferrite.

preferential formation of acicular ferrite at the expense of bainite. This at first sight appears to be consistent with the behaviour of the Fe-Cr-Mo-C welds, if it is assumed that the Cr and Mo prevent the formation of allotriomorphic ferrite at high concentrations and, hence lead to the promotion of classical bainite at the expense of acicular ferrite.

4.2 Experimentation

4.2.1 Alloy

The samples were machined from the all weld metal test specimen of alloy 78 (Table. 2.2). The samples were prepared as per the procedure outlined in chapter 2. The controlled heat treatments carried out on this alloy are presented below.

4.2.2 Furnace Heat Treatments

The main aim of the present investigation was to study the influence of prior allotriomorphic ferrite formation on the austenite/austenite grain boundaries, on subsequent transformation below B_s . To plan the heat treatments, a phase diagram and a time-temperature-transformation (TTT) diagram was calculated for the alloy 78, the calculation taking into account of the C, Si, Mn, Ni, Mo and Cr concentrations, using a method published elsewhere (Bhadeshia, 1981a, 1982a). The bainitic ferrite (B_s), Widmanstätten ferrite (W_s), and martensitic start temperatures (M_s) were also calculated using the same method (Fig. 4.1). The equilibrium Ae_3 transformation temperature was calculated as in Sugden and Bhadeshia (1989c). The transformation temperature data are presented in Table 4.1.

Table 4.1 Calculated transformation data for alloy 78.

Ae_3 , °C	838
W_s , °C	700
B_s , °C	578
M_s , °C	464

The experiments involved the isothermal reaction of austenite at two successive temperatures T_1 and T_2 . The heat treatment at T_1 was intended to allow the formation of some allotriomorphic ferrite, so that the austenite grain boundaries would be covered by a thin layer of the ferrite. The remainder of the austenite could then be transformed at a temperature T_2 below B_s . For comparison, the heat treatment at T_1 was omitted for some samples, the austenite being quenched directly to T_2 to avoid the formation of any allotriomorphic ferrite.

Table 4.2 Details of the furnace experiments:

Notation	T_γ °C	Time at T_γ min	T_1 °C	Time at T_1 min	T_2 °C	Time at T_2 minutes	Quench Condition
F1	1150	20	—	—	500	2	Ice+water
F2	1150	20	700	5	500	2	Ice+water
F3	1150	30	—	—	470	2	Ice+water
F4	1150	30	800	10	470	2	Ice+water
F5	1150	30	800	5	470	2	Ice+water
F6	1150	30	—	—	—	—	Continuous cooling †
F7	1150	30	800	10	600	2	Ice+water
F8	1150	30	800	10	—	—	Ice+water

†The cooling rate could not be measured as the samples were sealed in the quartz tubes, but was estimated to be about $50\text{ }^\circ\text{C s}^{-1}$.

Based on the data from the calculated TTT diagram, heat treatments F1 and F2 were planned as described in Table 4.2; the prefix F refers to experiments carried out using a resistance heated furnace. Three furnaces were maintained at the required temperatures one for austenitising at a temperature T_γ and the remaining ones for isothermal heat treatments at T_1 and T_2 . During the heat treatments, the samples were transferred rapidly between furnaces. Preliminary studies revealed that owing to relatively low cooling rate associated with such transfers, allotriomorphic ferrite formation could not be avoided in specimen F1 while cooling from T_γ to T_2 . In addition, heat treatment at $T_1 = 700\text{ }^\circ\text{C}$ was found to lead to the rapid growth of allotriomorphic ferrite to a very large volume fraction ($\simeq 0.75$) after only five minutes at T_1 . This defeats the purpose of the experiment, which was to decorate the austenite grain surfaces with *thin* layers of ferrite which do not consume the bulk of the austenite, leaving it free to decompose into intragranularly nucleated acicular ferrite.

To overcome these difficulties, the driving force for allotriomorphic ferrite growth was reduced by raising T_1 , and the cooling rate from T_1 to T_2 was increased by increasing further the difference $T_1 - T_2$ by reducing T_2 to $470\text{ }^\circ\text{C}$. These changes are not sufficient in themselves to prevent the formation of allotriomorphic ferrite in the interval between T_1 and T_2 , but that is not important, providing a thin covering of allotriomorphic layer is observed at the austenite grain

surfaces before T_2 is attained. The calculated data on the transformation behaviour expected for the present alloy (see Table 4.3), also suggest the scale of incubation time available at that particular temperature. The modified experiments (F3-F8) gave some results of interest which will be discussed below. The heat treatment schedules are shown schematically in Fig. 4.2

Table 4.3 Phase Diagram and TTT diagrams details at selected temperatures.					
Temp °C	$x_c^{\gamma\alpha}$	$x_c^{\alpha\gamma}$	\underline{D} cm ² s ⁻¹	α_1 cm s ^{-0.5}	τ s
800	0.0029	0.00042	0.117×10^{-7}	0.262×10^{-4}	0.51×10^4
760	0.0073	0.000542	0.7628×10^{-8}	1.526×10^{-4}	0.26×10^2
720	0.0150	0.000633	0.4416×10^{-8}	2.204×10^{-4}	0.5×10^1
680	0.0251	0.000698	0.2375×10^{-8}	2.321×10^{-4}	0.43×10^1
640	0.0362	0.000738	0.1291×10^{-8}	2.157×10^{-4}	0.88×10^1
600	0.0483	0.000754	0.0668×10^{-8}	1.838×10^{-4}	0.39×10^2

$x_c^{\gamma\alpha}$ is the carbon concentration in austenite which is in paraequilibrium with ferrite at the temperature concerned, in units of mole fraction

$x_c^{\alpha\gamma}$ is the carbon concentration in ferrite which is in paraequilibrium with austenite at the temperature concerned, in units of mole fraction

α_1 one-dimensional parabolic thickening rate constant for paraequilibrium growth of allotriomorphic ferrite

τ is the incubation time needed for detectable degree of transformation to ferrite from austenite.

\underline{D} is the weighted average diffusivity calculated by considering the carbon concentration profile in front of the moving ferrite interface, as discussed before (section 1.2.3)

4.2.3 Dilatometry

The dilatometric experiments were directed towards the investigation of the “incomplete reaction phenomenon” of the type reported for acicular ferrite and bainite in weld alloys, by Yang and Bhadeshia (1987a) and Strangwood and Bhadeshia (1987a). This would help to verify that the transformation products which form at T_2 correspond to the reported thermodynamic characterisation of bainite or acicular ferrite. Samples were austenitised at two different temperatures (1000 °C for 10 minutes or 1150 °C for 10 minutes) to obtain a small or a large

austenite grain size to induce a predominantly bainite or acicular ferrite microstructure, respectively, when subsequently transformed isothermally below the calculated B_s temperature. Thus, the experiment was designed to change the relative number densities of austenite grain boundary versus intragranular nucleation sites. Some details of the dilatometric experiments are given in the Table 4.4. Dilatometric relative length change data was analysed to obtain volume fractions of transformation. The method outlined in section 2.3 was adopted.

Table 4.4 Experimental details for the dilatometric tests:

Experiment Notation	T_γ °C	Time at T_γ seconds	T_i °C	Time at T_γ minutes	T_s °C	Δt_{850-T_i} seconds	Cooling condition
S1	1000	600	505	60	774	4.5	Quench
S2	1000	600	519	60	785	5.3	Quench
L1	1150	600	513	60	660	7.6	Quench
L2	1150	600	529	60	665	14.8	Quench

L,S denote the transformation from large and small austenite grain sizes respectively. The grain sizes measured for low T_γ and high T_γ samples were $41 \pm 5 \mu\text{m}$ ($T_\gamma=1000^\circ\text{C}$), $71 \pm 6 \mu\text{m}$ ($T_\gamma=1150^\circ\text{C}$) respectively as measured using the thermal grooving method.

4.2.4 Measurement of the linear thermal expansion coefficients

It is evident that a knowledge of the thermal expansion coefficients e_α and e_γ is necessary for computing the volume fraction of transformation as a function of the dilatometric length change. To measure the expansion coefficient of ferrite, dilatometer specimens were first tempered for one hour at 600°C to ensure an essentially ferritic microstructure. The length change data recorded during slow heating to 600°C and cooling from 600°C ($\approx 4^\circ\text{C s}^{-1}$) were then analysed to estimate the linear expansivity.

For austenite, length change data during heating from 850 to 1000°C , at a rate of 10°C s^{-1} , in the austenite phase field were analysed. The expansion coefficients measured in this way (Fig. 4.3) were found to be:

$$e_\alpha = 1.4026 \times 10^{-5} \pm 0.35 \times 10^{-7} \text{ }^\circ\text{C}^{-1} \text{ and } e_\gamma = 1.8854 \times 10^{-5} \pm 0.12 \times 10^{-7} \text{ }^\circ\text{C}^{-1}.$$

These values were constant over the temperature ranges studied, as indicated by correlation coefficients greater than 0.99 when the length change versus temperature data were subjected